Subcycle Fatigue Crack Growth Formulation

for Constant and Variable Amplitude Loading

by

Karthik Rajan Venkatesan

A Thesis Presented in Partial Fulfillment
of the Requirements for the Degree
Master of Science

Approved July 2016 by the
Graduate Supervisory Committee:

Yongming Liu, Chair
Hanqing Jiang
J.Oswald

ARIZONA STATE UNIVERSITY

August 2016

ABSTRACT

A previously developed small time scale fatigue crack growth model is improved, modified and extended with an emphasis on creating the simplest models that maintain the desired level of accuracy for a variety of materials. The model provides a means of estimating load sequence effects by continuously updating the crack opening stress every cycle, in a simplified manner. One of the significant phenomena of the crack opening stress under negative stress ratio is the residual tensile stress induced by the applied compressive stress. A modified coefficient is introduced to determine the extent to which residual stress impact the crack closure and is observed to vary for different materials. Several other literature models for crack closure under constant loading are also reviewed and compared with the proposed model. The modified model is then shown to predict several sets of published test results under constant loading for a variety of materials.

The crack opening stress is formalized as a function of the plastic zone sizes at the crack tip and the current crack length, which provided a means of approximation, accounting for both acceleration and retardation effects in a simplified manner. A sensitivity parameter is introduced to modify the enlarged plastic zone due to overload, to better fit the delay cycles with the test data and is observed to vary for different materials. Furthermore, the interaction effect induced by the combination of overload and underload sequence is modeled by depleting the compressive plastic zone due to an overload with the tensile plastic zone due to an underload. A qualitative analysis showed the simulation capacity of the small time scale model under different load types. A good agreement between prediction and test data for several irregular load types proved the applicability of the small time scale model under variable amplitude loading.

ACKNOWLEDGMENTS

I would like to thank Dr. Yongming Liu for guiding me through the study that is contained in this thesis work and also for the time he took to discuss all the important and challenging issues with me.

I would also like to thank all graduate students from the Prognostic and Reliability Assessment Lab, who, in any sense, participated and helped me in my research work. I would also like to thank members of my thesis committee - Dr. Hanqing Jiang, and Dr. J. Oswald, for taking the time to review my work.

The work is partially sponsored by NSF (1536994, Program Officer: Y. Grace Hsuan) and the financial support is greatly appreciated.

TABLE OF CONTENTS

LIST OF TABLES

LIST OF FIGURES

Chapter 1

INTRODUCTION

1.1 Objective

The main emphasis of this thesis work is on creating the simplest models for the crack growth rate process, of both constant and the random amplitude loading, that maintain the desired level of accuracy and efficiency. A new fatigue crack growth model, which combines some of the features of an existing model based on the time scale, is introduced and shown to predict several sets of published test results for different materials. The objective of this thesis could be summarized as

- To modify and extend the small time scale model to predict crack growth rate under tension-tension cyclic loading for a wide range of materials.
- To investigate the influence of the compressive stress cycles within a tension-compression cyclic loading on crack propagation rate.
- To develop a model for predicting crack opening stress level for different materials.
- To assess the retardation in crack propagation due to an overload and modify a suitable parameter for predicting the growth rate delay for different materials.
- To develop a model for predicting crack opening stress level that accounts for load interaction effect within variable amplitude loading.

The proposed modifications on FCGR models have been verified by applying the developed models to a variety of loading spectrum, thus verifying the integrity of the models and their applicability to a wide range of metallic alloys. To begin with, a brief review of the state of art is covered in the next section in this chapter.

1.2 Background and literature review

1.2.1 Fracture Mechanics

A crack can be developed in a material due to many reasons. It may exist due to a manufacturing defect, due to application of load higher than the material's yield point; which may lead to fracture. As illustrated in Fig 1, a crack can experience three kinds of load types. The mode I Fig.1A would occur when load is applied perpendicular to the crack surface. Mode II Fig.1B and Mode III Fig.1C are mostly in plane and out of plane shear loading. In reality, a crack can be subjected to a combination of different load modes.

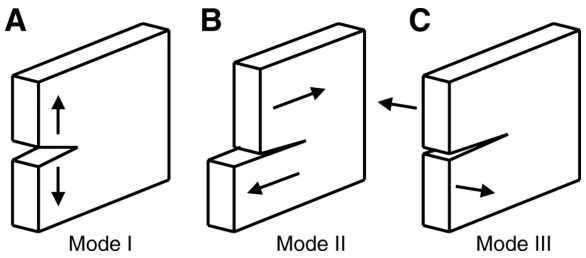

Figure 1. Different modes of fracture

The stress distribution ahead of the crack tip is usually defined by the parameter K termed as the stress intensity factor. In an infinite plate, the stress intensity factor K as a function of the applied stress σ, half crack length a is given as

$$K = Y\sigma\sqrt{\pi a} \tag{1.1}$$

Where Y is a geometry dependent parameter known as the geometric correction factor, which could be evaluated using finite element analysis. The geometric correction

factor in general is a function of the half crack length a and the half width W of a finite plate. For an infinite plate specimen, the value of Y is 1.

1.2.2 Fatigue Crack Growth Rate

Fatigue crack growth rate with respect to the applied stress intensity factor range is typically shown in a logarithmic scale, as illustrated in Figure 2, Crack propagation rates are different in each regions. In region I, the growth rate is in the order of 10^{-9} m/cycle or less. A crack would not propagate if the applied stress intensity factor range is lesser than the threshold value, K_{th}. Several research has been done in evaluating the K_{th} for different loading parameters and material strength. The second region is a linear logarithmic function of the applied stress intensity factor. Most of the research is done in this region, which accounts for the steady state propagation rate. As the crack reaches the third region, the growth rate accelerates and eventually ends with the specimen being fractured.

1.2.3 Constant Amplitude Loading(CAL)

Several models have been proposed for estimating the crack growth rate in the second region, under constant amplitude loading. The rate of crack growth is modelled as a function of the stress intensity factor K. Under CAL, the stress intensity factor range is a function of the applied stress range and the crack length and is given as

$$\Delta K = Y \Delta\sigma \sqrt{\pi a} \tag{1.2}$$

Under positive ratio, σ_{max} and σ_{min} are the maximum and minimum applied stress

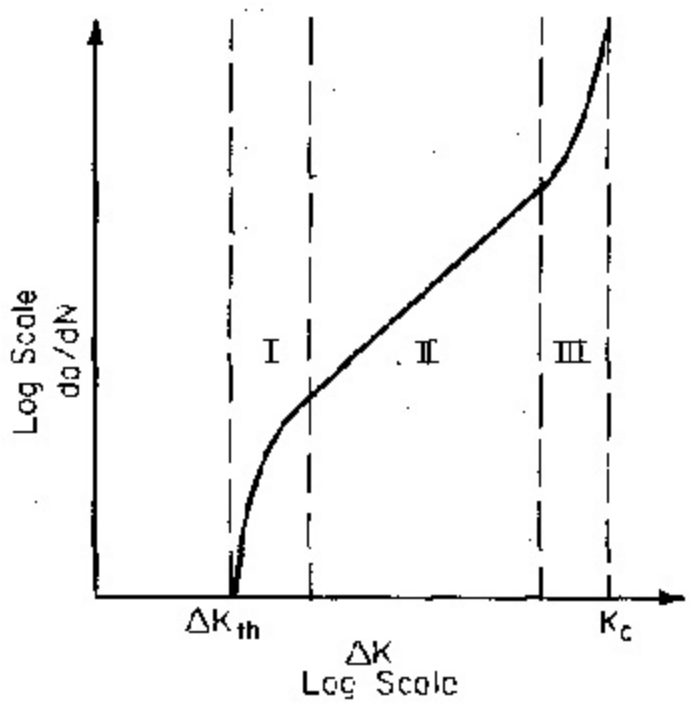

Figure 2. Crack propagation rate versus stress intensity factor range

in the load cycle. However under negative stress ratio, standards suggests that only the positive portion of the load cycle contributes to the crack propagation. In other words, the minimum stress σ_{min} is equal to zero and σ_{max} would contribute to the crack propagation. Some of the fatigue crack propagation models from the literature are discussed below.

In 1963, Paris andn Erdogan (Paris and Erdogan 1997) proposed the model which is known as the Paris model given by the equation

$$\frac{da}{dN} = C\Delta K^m \tag{1.3}$$

where C and m are curve fitting parameters known as Paris constants that can be established with experimental data. The Paris model typically describes the second region of the fatigue growth rate curve as shown in Fig. The constant C represents the intercept of the line and m represents the slope of the line. Hence, the limitation

being that the model can predict only in the second region. Also, the model does not account for different stress ratios in the load cycle.

Unlike Paris law, the Forman model (Walker 1970) considers the influence of stress ratio and also has the capability to predict in both region II and region III of the fatigue growth rate curve. It is given by the following equation

$$\frac{da}{dN} = \frac{A^{'}(\Delta K)^{n'}}{(1-R)(K_c - K_{max})} \tag{1.4}$$

$A^{'}$ and $n^{'}$ are empirical material constants and K_c represents the fracture toughness of the material. The above equation is a modification of the Paris model that incorporates the fracture toughness K_c, which accounts for region III growth rate.

In 1970, Eiber (Elber 1997) showed that a fatigue crack remains closed during part of the load cycle and termed the mechanism as fatigue crack closure. He argued that as a result of tensile plastic deformation left in the wake of a fatigue crack tip, the crack faces remain partially closed until a minimum stress is reached. Since his argument, several research on his statement has been performed and documented. Several models have been later proposed to explain the crack closure concept. However, many details in the mechanism are only partly understood.

The crack opening stress is typically larger than the minimum stress, as illustrated in the Figure 3. At σ_{op} the crack tip fully opens and below σ_{min} the crack remains closed and does not propagate. He proposed that the effective stress intensity factor range ΔK_{eff} is the driving force parameter instead of the nominal stress intensity factor range ΔK. One parameter that is used to define the crack closure estimation is the closure ratio

$$U = \frac{\Delta K_{eff}}{\Delta K}, \tag{1.5}$$

where $\Delta K_{eff} = K_{max} - K_{op}$

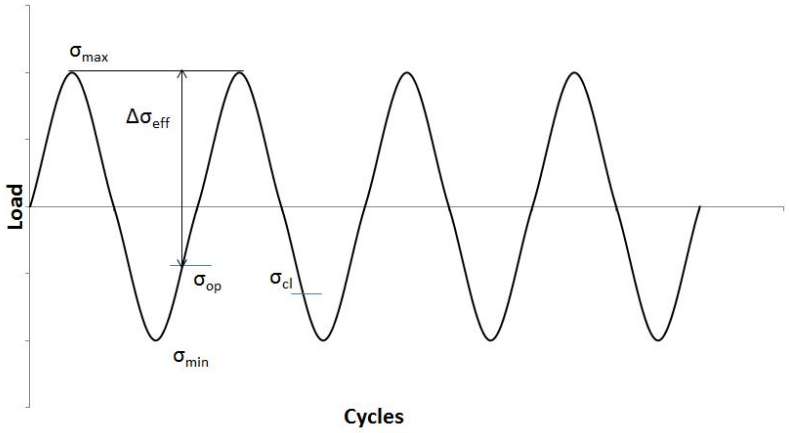

Figure 3. Schematic representation of load history with crack opening level

The significance of crack opening stress is usually related to the crack growth, retardation/acceleration, or arrest of fatigue cracks under load histories. The effect of crack opening level on several in-service load histories are presented in the coming chapters.

1.2.4 Variable Amplitude Loading(VAL)

In this subsection, fatigue crack growth behaviour observed under variable amplitude loading is briefly reviewed. A variable amplitude loading sequence can either accelerate or retard the fatigue crack growth rate which depends on a numerous factor. In general, the applied load, material strength, geometry of the specimen and other environmental conditions account for the extent to which the crack growth accelerates or retards from the steady state characteristics. Some of the physical arguments that have been implied to explain the load-interaction effect of fatigue crack growth rate are as follows

- Crack tip blunting

- Residual stress
- Crack tip plasticity
- Plasticity induced crack closure

A crack tip gets blunted by an overload, which makes it behave like a notch. This idea known as Crack tip blunting was first proposed by Christensen (Christensen 1959). The retardation is the number of cycles required for a crack to propagate from the notch and continue steady state characteristics. Some research study showed that both the retardation after a single overload and acceleration after underload were due to crack tip blunting. This however cannot explain the reason behind the initial acceleration immediately after an overload.

The residual stress theory (Schijve and Broek 1962) assumes that compressive residual stresses can be generated in the small region around the crack tip after an overload. The compressive residual stresses superimposed with the actual applied stresses gives the resultant effective stresses which becomes the driving parameter (Schijve and Broek 1962) for fatigue crack growth.

Crack tip plasticity models are based on the enlarged plastic zone size ahead of the crack tip. According to Wheeler (Wheeler 1972), the fatigue crack growth rate under the application of a single overload can be determined by introducing retardation parameter C_p to the Paris equation, which is as

$$\frac{da}{dN_i} = (C_p)_i[C(\Delta K_i)^m] \tag{1.6}$$

The retardation parameter C_p depends on the current plastic zone size, $r_{p,i}$, and the overload plastic zone size, r_{OL}. The subscript 'i' indicates the particular cycle in the load history.

$$(C_p)_i = \left(\frac{r_{p,i}}{r_{OL} - \Delta a_i} \right)^p \tag{1.7}$$

The limitation to the wheeler's model is the shaping exponent p, which has to be experimentally determined for each load history. Moreover, the crack growth acceleration due to underloads cannot be simulated using this model.

While eliminating the additional parameter such as C_p in the wheeler's model, Willenborg model (Willenborg, Engle, and Wood 1971) accounts for retardation after an overload by substituting the effective stress ratio, R_{eff} and the effective stress range, $\Delta\sigma_{eff}$, into the Forman Eq. (1.2). The actual stress intensity factor acting on the crack tip is assumed to be calculated based on the λ parameter as shown below

$$K_b = \sigma_y (R_{OL} \pi (a_o + r_{OL} - a))^{0.5} \tag{1.8}$$

where σ_y is the yield stress, R_{OL} is the overload ratio, a_o is the crack length when overload was applied, r_{OL} is the overload plastic zone size. Based on this, the residual stress intensity factor, K_{res} and effective stress intensity factor K_{eff} are calculated as

$$K_{res} = K_{max} - K_b \tag{1.9}$$

$$K_{eff} = K_{appl} - K_{res} \tag{1.10}$$

In recent study (Lee and Chen 2002), the Willenborg model has shown complete crack arrest when sufficiently high overload ratio is applied. Moreover, the model cannot predict delayed retardation, but only the immediate retardation right after an overload. The model cannot simulate underloads as the compressive loads are neglected by default in the FCG equation.

The concept of plasticity induced crack closure is to account for load-interaction effects by incorporation the effective stress intensity range, ΔK_{eff}. Several crack

opening models for constant loading were later modified to model under variable loading (Padmadinata 1990). The model proposed by Newmann is known to be a popular approach. According to this model, the crack opening stress differs for each level of applied stress and is calculated cycle by cycle basis. For simplicity, it is assumed (J. Newman 1982) that the crack opening stress σ_{op} for a given block of variable amplitude loading is constant. The crack opening stress can be estimated from the constant amplitude fatigue test data with the equivalent stress intensity range defined as $\Delta K = K_{max,VA} - K_{min,VA}$, where $K_{max,VA}$ and $K_{min,VA}$ are the maximum and minimum stress intensity factor in one block of variable amplitude loading (Suresh 1998).

$$\frac{da}{dN_i} = A(\Delta K_{eff,i})^m \tag{1.11}$$

Where $\Delta K = K_{max,i} - K_{op}$. The constant A is correlated using the Paris constant C using the following equation (Bannantine 1990)

$$A = \frac{C}{(U_i)^m} \tag{1.12}$$

where $U_i = \frac{\Delta K_{eff,i}}{\Delta K_{appl,i}}$

A numerical integration method is used to solve for N in Eq. (1.11) in order to obtain cycle by cycle crack growth increments from initial crack size to fracture. Several computer programs such as NASGRO, FASTRAN-2, MODGRO and FLAGRO have been developed based on this approach to estimate fatigue life under variable amplitude loading.

1.2.5 Small Time Scale Formulation

The small time scale model (Lu and Liu 2010) is based on the incremental crack growth at any instantaneous of time during a loading cycle. Compared to the conventional cycle-based approach, this model can be used for fatigue analysis at various time and length scales. This model is also very convenient for predicting FCG behavior under random variable amplitude loading. The model was developed by establishing a geometric relationship between the incremental crack growth da and the change in CTOD $d\delta$. Based on fracture Based on fracture mechanics, the theoretical relationship between CTOD and the SIF was used to correlate to the incremental crack growth. The crack extension Δa during a small time scale Δt was then calculated by direct integration. Based on this model, the crack growth in one load cycle is given as

$$a = AK_{max}\sqrt{\delta} \tag{1.13}$$

Where A is a fitting parameter. The CTOD remains unchanged below crack closure and is a function of effective SIF. The analytical approximation of the CTOD (Liu, Lu, and Xu 2012) at that instantaneous of time is given as

$$\delta = \frac{{\Delta K_{eff}}^2}{2E\sigma_y} \tag{1.14}$$

E and σ_y are the Young's modulus and material yield strength.

The analytical approximation for crack tip opening displacement under variable amplitude loading was derived in the same paper. The CTOD was observed to vary based on the memory variable $K_{max,mem}$, which specifies the maximum SIF corresponding to the largest monotonic plastic zone size in the variable load history.

The model predictions had good agreement with experimental observations for Al 2024-T3 and Al 7075-T6. The predictions were compared with those of FASTRAN and AFGROW codes, and an overall better accuracy is observed when investigated for both uniform tension-tension and random amplitude loading. However, the model is incapable of simulation crack growth propagation under negative stress ratio and lacked applicability for other metallic materials.

1.3 Summary and Conclusion

Some of the common fatigue crack propagation models have been reviewed in this chapter. Crack propagation under constant amplitude loading would typically be a power function of the stress intensity factor range ΔK. Loading interaction effect should be considered when predicting the fatigue life under variable amplitude loading. Several crack propagation models are proposed to predict the growth rate under CAL. The model coefficients are usually evaluated using experimental results.

Under variable amplitude loading, loading interaction has a significant effect on the crack growth rate. On application of a tensile overload, the FCGR retards while on a compressive underload, the FCGR would be faster. Few models were reviewed that account for the load-interaction effect. It is noticeable that most of the models are based on the size of the plastic zone developed ahead of the crack tip.

The small time scale model formulation has been reviewed which is the fundamental basis for this research study. The model is later modified and extended to predict crack growth rate under negative stress ratio and variable amplitude loading for a wide range of materials.

Chapter 2

FATIGUE CRACK GROWTH UNDER CONSTANT AMPLITUDE LOADING

2.1 Overview

Under tension-compression loading, the calculation of ΔK is usually based on the stresses in the tensile part of the fatigue loading and the contribution from the compressive load is ignored. This is based on the assumption that under applied compressive stress, the crack tip is closed and no stress intensity factor is associated with the crack. Although the crack will be closed within the compressive load region, FCG is strongly affected by the local plastic deformation at the crack tip region (Chen et al. 2015). Several literature results based on tests performed under tension-compression fatigue loading indicates that the effect of compressive load on FCG was strongly material dependent (J.-z. Zhang et al. 2010). In the literature, different empirical models for crack closure have been proposed for both positive and negative ratios. Several empirical models and models based on finite element analysis have been proposed for estimating crack closure stress for negative stress ratio. Newman (J. J. Newman 1984), Lang (Lang 2000), Schijve (Schijve 1981), de Koning proposed empirical expressions for crack opening stress level which also included negative stress ratios. However, less effort has been made in the understanding of fatigue crack closure under tension-compression loading. In this chapter, the FCG behavior of different materials subjected to various stress ratios is investigated. The integrity of the existing model based on the small time scale concept (Lu and Liu 2010) with the current crack closure model is studied, and their results are discussed. The predictions agreed

well with experimental observations for Al 2024-T3 and Al 7075-T6 Aluminum alloy under tension-tension fatigue loading. The small time scale model was modified to predict FCGR for 4340 Steel and Magnesium alloy. From the perspective of plasticity induced crack closure (PICC), the objective here is to study the effect of compressive stress and the applicability of PICC to explain the impact of material yield strength on crack closure at negative stress ratios. Finally, a crack closure model, developed based on virtual crack annealing technique and the collected experimental data, is presented. The model is capable of accounting for a wide range of stress ratios and different loading scenarios, effectively for various materials in the time scale.

2.2 Modified Small Time Scale Model

The small time scale model predictions agreed well with experimental data for Al 2024 and 7075 Aluminum alloys. The model is amended to predict FCG behavior for positive stress ratios for 4340 Steel, Ti-6Al-4V and AM60B as well. In order to achieve this, a power fit parameter B is introduced to the small time scale FCG equation. The modified relation is given as

$$a = AK_{max}^{B}\sqrt{\delta} \tag{2.1}$$

The parameters A and B are calculated to match the intercept and the slope with that of the experimental data. Experimental data at $R = 0$ is considered as the baseline and the Paris's constants for each material are calculated and presented in Table 1.

The crack growth rate from the Paris's law is compared with the small time scale

Table 1. Summary of Paris model constants for each material

Material	C	m	E	σ_y
AM60B Mg alloy	1.57E-10	3.87	40000	150
2024-T3 Al alloy	5.10E-12	3.67	71700	315
D16 Al alloy	3.39E-10	2.51	72000	345
Al 7075-T6 Al alloy	5.62E-11	3.29	69600	520
Ti-6Al-4V alloy	1.02E-11	3.303	117000	1185
4340 Steel	2.00E-11	2.51	200000	1410

model and the fitting parameter A and B are calculated as

$$\left| A = \frac{2C\sqrt{2E\sigma_y}}{U}, \right| B = m - 2 \tag{2.2}$$

Based on this, the FCG Eq (2.1) is modified and the fitting parameter for each material is presented in Table 2.

Table 2. Summary of model fitting parameter for each material

Material	A	B
AM60B Mg alloy	1.99E-06	2.87
2024-T3 Al alloy	1.25E-07	2.67
D16 Al alloy	7.99E-06	1.51
Al 7075-T6 Al alloy	1.75E-06	2.29
Ti-6Al-4V alloy	5.68E-07	2.303
4340 Steel	1.73E-06	1.51

The applicability of the small time scale model with the present model for crack closure for the above materials is tested for a broad range of stress ratios.

2.3 Virtual Crack Annealing Model for Crack Closure

2.3.1 Existing model for Positive stress ratio

A previously developed mechanical model for crack opening stress is considered for the study. This model is based on the approximation that the crack surface behind the crack tip is fully closed during the cyclic loading. This model was developed for constant amplitude loading. The model assumes that the CTRPZ and the CTOD change until the crack closure happens. The crack opening stress (Zhang and Liu 2012) for a fixed maximum load σ_{max} is given as

$$\sigma_{op}/\sigma_{max} = 0.4 + 0.6R \tag{2.3}$$

Where stress ratio $\sigma_{min}/\sigma_{max}$ and σ_{op} is the crack opening stress in one load cycle. Based on this model, the portion of load cycle during which the crack is fully open is given as

$$U = \frac{\Delta K_{eff}}{\Delta K} = 0.6 \tag{2.4}$$

The virtual crack annealing method for crack closure calculation has been discussed in the next section. One limitation of this model is that it is applicable only for positive R-values, i.e., the applied minimum stress σ_{min} is with in the tension part of the cyclic loading.

2.3.2 Proposed Model for Negative Stress Ratio

For ease of discussion, a crack under uniform tension-compression fatigue loading (Fig. 4) is discussed first. If the crack is unloaded from its maximum current loading, the crack remains open initially. The reverse plastic zone and the CTOD change until

crack closure. However, on further unloading to a maximum applied compressive stress, the size of reverse plastic zone increases with the rise in reversed plastic deformation (Antunes et al. 2015) until both the crack faces come in contact with each other. Beyond the contact stress level, the RPZ cannot be calculated using classical fracture mechanics. However, the effect of the CTRPZ on fatigue crack closure after crack surface contact occurs is assumed to be negligible. A simple analytical approximation is proposed in this paper which assumes that there exists two closure levels during a tension-compression cyclic loading. One is the partial crack closure due to unloading and the other one is termed as global contact closure due to application of remote comrpessive load.

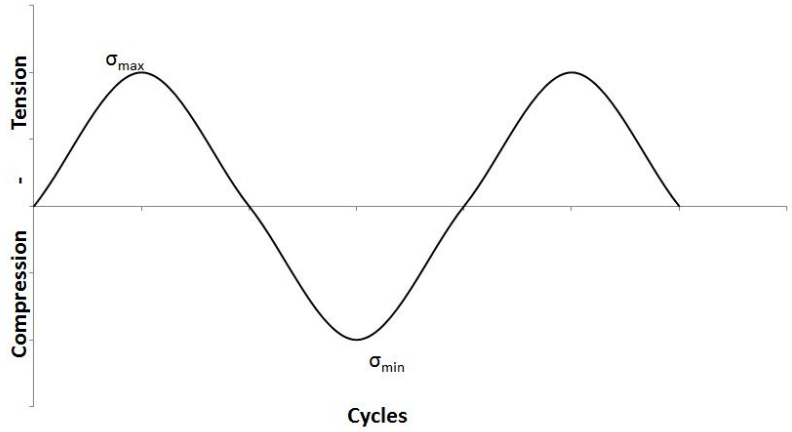

Figure 4. Tension-compression fatigue loading

2.3.2.1 Model Illustration

In order to illustrate the basic idea of this model, a schematic representation is shown in Fig. 5. A real crack after unloading from a maximum tensile stress is shown in Fig. 5 (a). The length of the crack is a and the closure length is d. The crack tip

reversed plastic zone d_r (CTRPZ) is filled with compressive residual stress, with the stresses transferring through the crack surface in the crack closure zone d. Using the assumption of virtual crack annealing, a virtual crack of length (a-d) and a reversed plastic zone size of $(d + d_r)$ can be assumed. When the compressive residual stress with in the distance d ahead of the crack tip becomes zero, the crack is fully open. The real crack and the virtual crack are equivalent in the sense that both have the same diameter of residual stress zone. For the real crack, the RPZ considering crack closure can be expressed as,

$$d_r = \frac{\pi}{8}\left(\frac{K_{max} - K_{cl}}{2\sigma_y}\right)^2 \tag{2.5}$$

If the virtual crack with a crack length (a-d) of is under the same loading conditions, classical fracture mechanics can still be applied to calculate the reversed plastic zone until the global crack surface contact occurs. To depict this, a global contact stress σ_{gc} is assumed to control the size of the reversed plastic zone for the virtual crack which can be expressed as

$$d_{r,virtual} = \frac{\pi}{8}\left(\frac{K_{max} - K_{gc}}{2\sigma_y}\right)^2 \tag{2.6}$$

Where K_{cl} ,σ_{cl} and K_{gc} ,σ_{gc} are the SIF and stress level at the crack closure and global crack contact.

From Fig. 5(a) and Fig. 5(b), the overlapped length d can be estimated as

$$d = d_{r,virtual} - d_r = \frac{\pi}{8}\left(\frac{\sigma_{max} - \sigma_{gc}}{2\sigma_y}\right)^2 \pi(a-d) - \frac{\pi}{8}\left(\frac{\sigma_{max} - \sigma_{cl}}{2\sigma_y}\right)^2 \pi(a) \tag{2.7}$$

Now consider the virtual crack under reloading from applied remote compressive stress to maximum tensile stress. Upon reloading, the overlapped length will gradually reduce to zero until a certain stress level σ_{op}. Also, the stress at the overlapped length

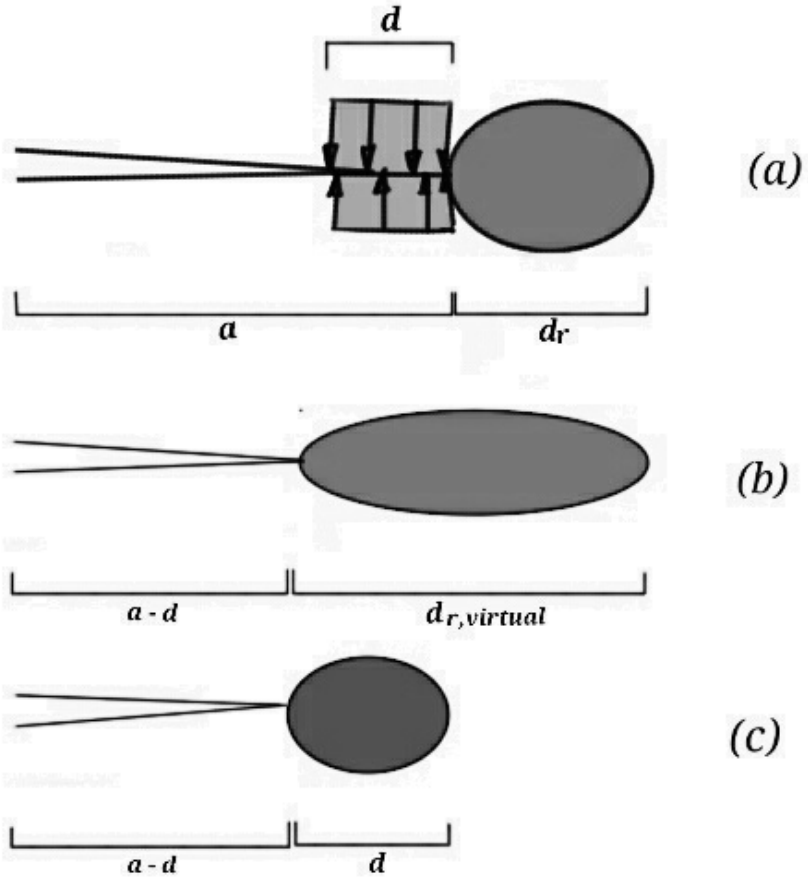

Figure 5. Schematic representation of (a) Real crack after unloading from σ_{max}, (b) Virtual crack, (c) Crack during reloading from σ_{min}

will change from $-\sigma_y$ at the global crack contact stress σ_{gc} to zero at the full open stage σ_{op}. Based on this concept, the forward plastic zone of the virtual crack at the

opening stress will be equal to the overlapped length and can be expressed as

$$d = \frac{\pi}{8}\left(\frac{\sigma_{op} - \sigma_{gc}}{\sigma_y}\right)^2 \pi(a-d) \tag{2.8}$$

As a first order approximation, the crack opening stress and the closure stress in one load cycle are assumed to be identical. Also, the material is assumed to be perfect elastic plastic and a factor of 1 for no significant hardening is assumed as a good estimate. Under this hypothesis, the analytical approximation of crack opening can be obtained by combining Eq (2.7) and Eq (2.8).

$$\frac{\pi}{8}\left(\frac{\sigma_{max} - \sigma_{gc}}{2\sigma_y}\right)^2 \pi(a-d) - \frac{\pi}{8}\left(\frac{\sigma_{max} - \sigma_{op}}{2\sigma_y}\right)^2 \pi(a) = \frac{\pi}{8}\left(\frac{\sigma_{op} - \sigma_{gc}}{\sigma_y}\right)^2 \pi(a-d) \tag{2.9}$$

Assuming that the closure overlapped length is smaller than the actual crack length and its effect on SIF is negligible, Eq (2.9). can be further simplified as

$$5\sigma_{op}^2 - (8\sigma_{gc} + 2\sigma_{max})\sigma_{op} + (3\sigma_{gc}^2 + 2\sigma_{max}\sigma_{gc}) = 0 \tag{2.10}$$

$$(\sigma_{op} - \sigma_{gc})(5\sigma_{op} - 2\sigma_{max} - 3\sigma_{gc}) = 0 \tag{2.11}$$

The above equation gives two possible solutions to crack opening stress level. One solution is that $\sigma_{op} = \sigma_{gc}$, which indicates that the crack opening stress is compressive and that the tensile peak load has no effect on crack closure. The other solution gives a unique crack closure level under constant tension-compression loading that can be expressed as

$$\sigma_{op} = 0.4\sigma_{max} + 0.6\sigma_{gc} \tag{2.12}$$

The objective here to estimate the global contact stress, which can be utilized to correlate the extent to which reversed plastic deformation occurs in the compressive part of the fatigue loading.

2.3.2.2 Effect of Compressive Stress Level

During unloading, the compressive stress produces reversed plastic deformation, which is known to reduce the crack opening stress level. With the decrease in minimum stress, while fixing the maximum stress, the reversed plastic deformation at the crack tip increased, this was observed by F.V. Antunes(Antunes et al. 2015). A linear variation of the size of the RPZ at the crack tip can also be expected with the increase of compressive load, which was observed in the paper (Zhang, He, and Du 2007). In the previous section, the size of the reversed plastic zone is assumed to depend on the global contact stress, under the hypothesis that the reversed plastic zone cannot increase beyond crack surface contact. To depict this, a non-dimensional parameter β was introduced to scale the effect of different peak compressive load σ_{min} on the global crack face contact stress under small-scale yielding.

$$\sigma_{gc} = \beta\sigma_{min} \tag{2.13}$$

Substituting Eq (2.13) in Eq.(2.12), the crack opening stress as a fraction of applied maximum stress can be given as

$$\sigma_{op}/\sigma_{max} = 0.4 + 0.6\beta R \tag{2.14}$$

To explain the effect of compressive stress on the global contact stress, the obtained relation for crack opening stress is applied to the small time scale model for crack growth rate and is analyzed using literature results of fatigue crack growth rate at negative stress ratios. The scaling parameter β is calculated by calibrating the model with experimental data.

From the literature results, the value of ΔK at $da/dN = 10^{-6}$ mm/cycles has been derived here (see Table 3) for three different materials. Since the opening stress

was observed to have a linear trend with the increase in σ_{min}, only one set of data at negative stress ratio is considered to capture the trend for each material.

Table 3. Scaling parameter β for different materials

Material	R	ΔK	U	β
2024-T3 Al alloy	-1	11.628	0.35639	0.187
Al 7075-T6 Al alloy	-1	8.594	0.34642	0.154
4340 Steel	-1	21.684	0.32942	0.098

The crack growth rate function for small time scale is obtained by differentiating Eq.(2.1) with respect to time and is given as

$$da = \frac{A{K_{max}}^B d\delta}{2\sqrt{\delta}} \tag{2.15}$$

Assuming the CTOD variation is constant under constant amplitude loading, the simplified form the above equation is as

$$da = \frac{A}{2}\frac{{K_{max}}^B \Delta K_{eff}}{2E\sigma_y} \tag{2.16}$$

Crack opening stress as a fraction of peak tensile load can also be expressed as

$$\sigma_{op}/\sigma_{max} = 1 - U(1-R) \tag{2.17}$$

Where U is the fraction of the load cycle during which the crack is open and is obtained by combining Eq. (1.2), Eq. (2.4) and Eq. (2.16) as follows

$$U = \Big(\frac{da(1-R)^B\sqrt{2E\sigma_y}}{A\Delta K^2}\Big)^{0.5} \tag{2.18}$$

From Eq. (2.17) and Eq. (2.14), the scaling parameter β can be expressed as

$$\beta = \frac{0.6 - U(1-R)}{0.6R} \tag{2.19}$$

By substituting the values for U and the corresponding stress ratio R, the parameter β is calculated and observed to vary for different materials.

2.3.2.3 Effect of Material Yield Strength

Based on the previous section, the parameter β was calculated and found to vary for different materials. Fig 6 plots β for materials with different yield strength. The closure load at R = -1 is calculated for each material by Eq. (2.18) and is observed to increase with the increase in yield strength for different materials.

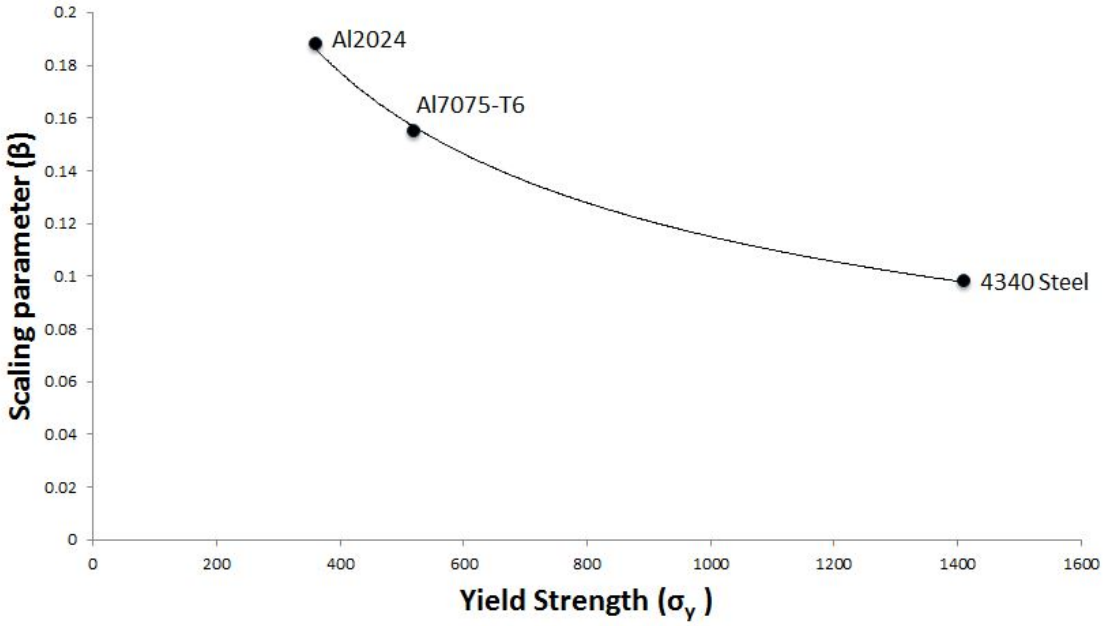

Figure 6. Parameter β as a function of yield strength for three materials

A non-linear function is fit to capture the trend in which β varies for different yield strength and is give as

$$\beta = \frac{3.06}{\sigma_y^{0.472}} \tag{2.20}$$

A discussion of this solution is given in the next section by comparing with other models for crack closure at negative stress ratio. The modified virtual crack annealing

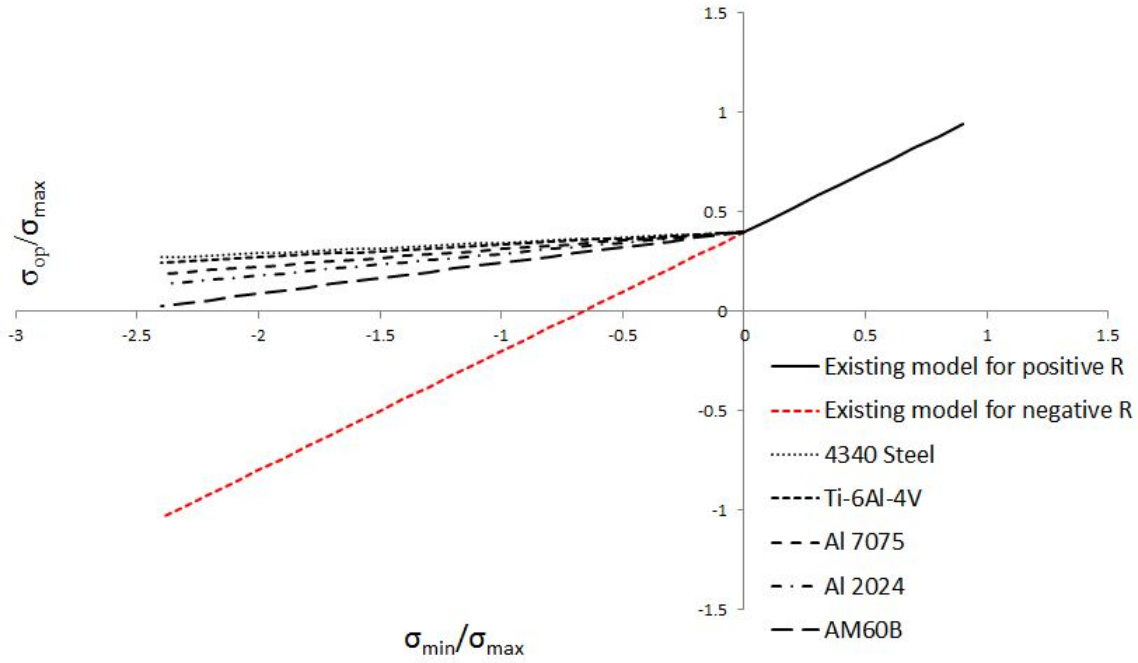

Figure 7. Model prediction for crack opening stress as a function of stress ratio

model is then used to formulate the fatigue crack growth behavior under variable amplitude loading (VAL).

2.4 Discussion

The proposed empirical model for fatigue crack closure at negative stress ratio accounts for the effect of loading parameters and yield stress. However, Plasticity induced crack closure is the only mechanics considered in this model. Further development may be required to include other parameters. The model presented is fascinating to study the effect of loading parameters and the effect of yield strength on crack closure at negative stress ratio. Figure 8 plots the σ_{op}/σ_{max} against σ_y for different negative stress ratios.

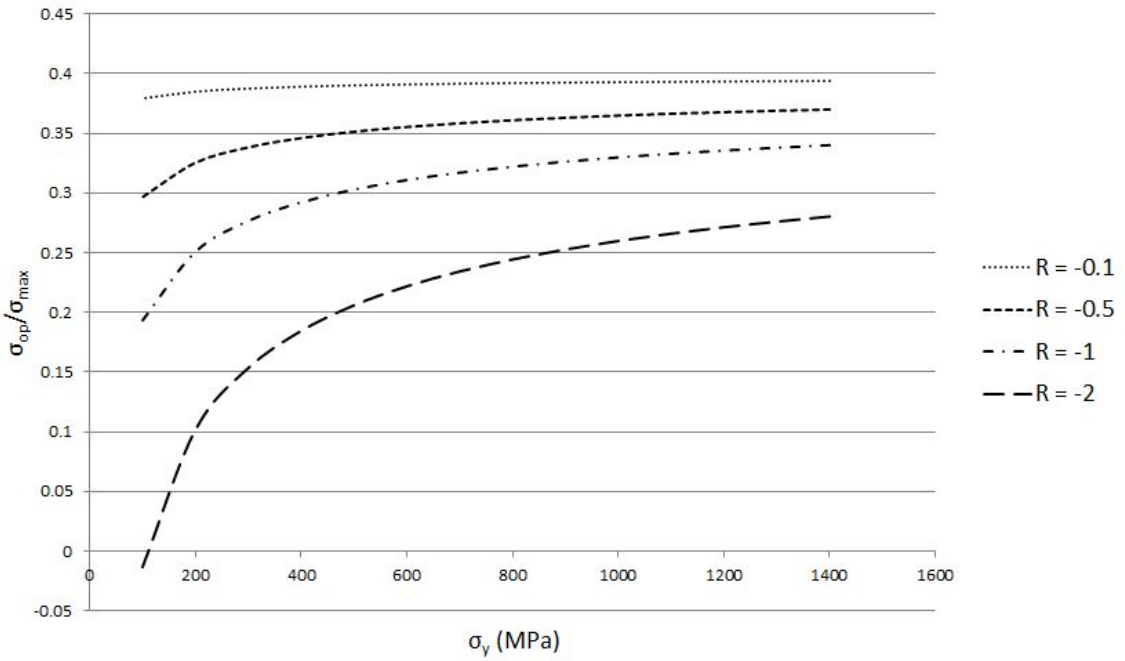

Figure 8. Empirical model: Effect of yield stress σ_y on crack closure at negative stress ratio

Table 4. Summary of literature models for σ_{op} as a function of stress ratio

Author	σ_{op}/σ_{max}	Material	Validity R
(Elber 1997)	$0.5 + 0.1R + 0.4R^2$	2024-T3	-0.1 to 0.7
(Schijve 1981)	$0.45 + 0.22R + 0.21R^2 + 0.12R^3$	2024-T3	-1 to 0.5
(S. Zhang et al. 1987)	$(0.38 + 0.36R + 0.14R^2)(1 - R)$	7475-T73	-1 to 0.5
(Kumar 1995)	$(0.3 + 0.15R(2 + R))(1 - R)$	Steel	-1 to 0.5
(Lang 2000)	$0.45 + 0.34R + 0.13R^2 + 0.07R^3$	7475-T7351	-0.7 to 1
(J. J. Newman 1984)	$0.53 + 0.07R + 0.14R^2 + 0.25R^3$	7075-T6	-1 to 0.9

The plot 9 shows the crack opening stress as a function of stress ratio for different empirical models obtained from the literature. The value of σ_{op} decreases with stress ratio. The variations in σ_{op} for negative stress ratio is moderate compared to positive stress ratio. Different materials were considered to generate these models. Hence, a significant difference in the value of σ_{op} is observed although the global trend presented by the different literature models is similar. The plot 10 shows the crack opening stress

σ_{op} against stress ratio for different values of yield strength σ_y, using the empirical model proposed here Eq (2.18).

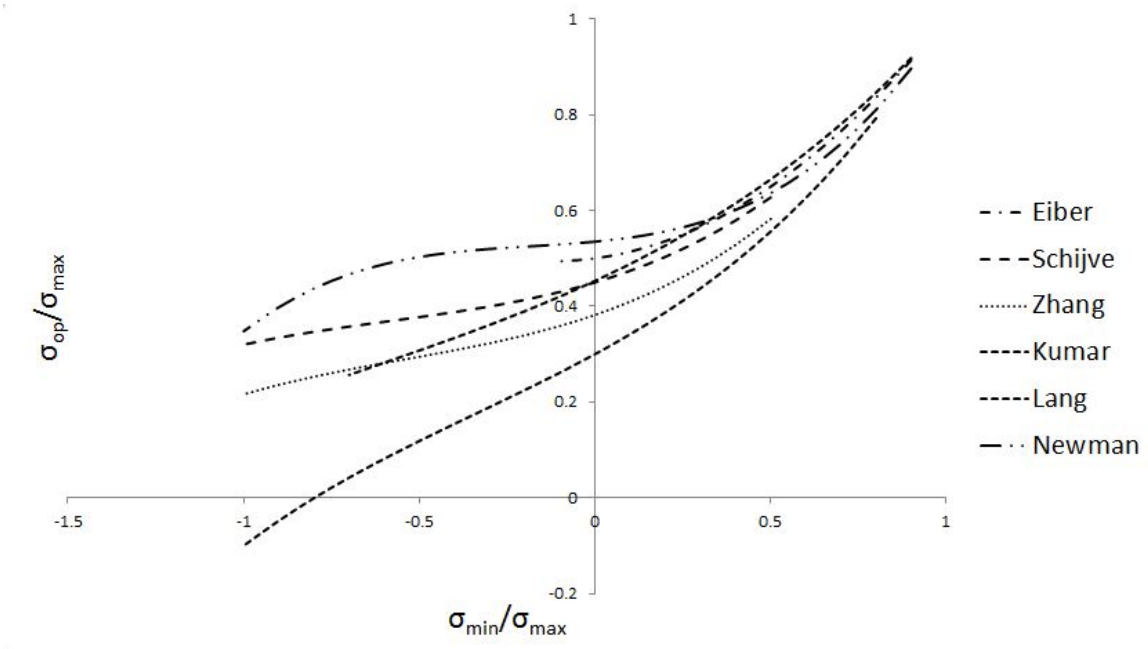

Figure 9. Comparison of literature models for closure ratio as a function of stress ratio

For positive stress ratio, the closure loads are not dependent on the material yield strength. However, there is a significant influence of σ_y and its decrease decreases the crack opening level σ_{op} for negative stress ratio. The comparison of plots in 9 and 10 indicates similar trends and similar crack opening values. The scatter observed for negative stress ratio in Fig 9 compared to Fig 10 may be explained by loading parameters and different material yield strength.

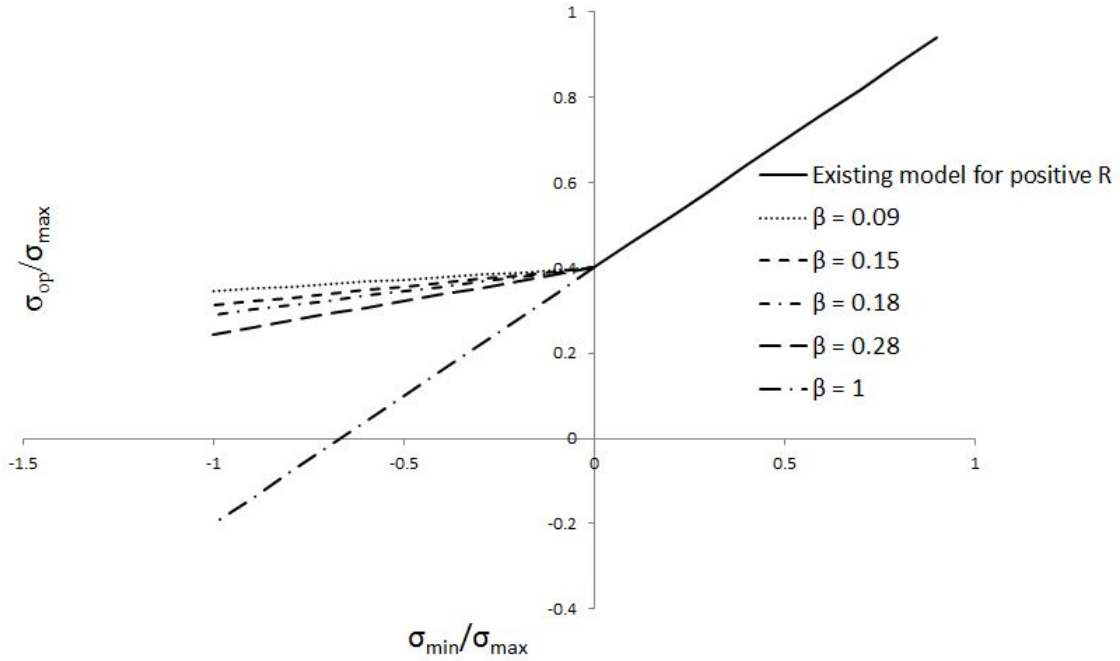

Figure 10. Model predictions for closure ratio as a function of stress ratio for different yield strength

2.5 Model Validation

In order to demonstrate the validity of the fatigue crack growth formulation presented above, its predictions are compared to the test date for different materials. Fatigue test data under constant amplitude loading for Aluminum alloy 7075-T6 and 2024-T3, 4340 Steel, Ti-6AL-4V Titanium alloy and AM60B Magnesium alloy,are used to validate the present model. Figure. 11 to 15 plots experimental fatigue data obtained from the literature. A summary of the model parameters calculated for each material is given in Table 5 below. The test data obtained from the literature are cited next to the corresponding material in Table 5.

Table 5. Summary of model parameters for each material

Material	A	B	E	σ_y	β
AM60B Mg alloy	1.99E-06	2.87	40000	150	0.284
2024-T3 Al alloy	1.25E-07	2.67	71700	315	0.187
D16 Al alloy	7.99E-06	1.51	72000	345	0.179
Al 7075-T6 Al alloy	1.75E-06	2.29	69600	520	0.154
Ti-6Al-4V alloy	5.68E-07	2.303	117000	1185	0.10
4340 Steel	1.73E-06	1.51	200000	1410	0.098

Table 6. Summary of test data for different metallic materials under different stress ratio

Material	Stress ratio R	Reference
AM60B Mg alloy	0, 0.25, 0.5, -0.3, -0.6, -1.0	(Mehrzadi and Taheri 2012)
2024-T3 Al alloy	0 , 0.1, 0.3, 0.5, -0.5, -1, -2	(Forman et al. 2005)
Al 7075-T6 Al alloy	0, 0.33, 0.75, -0.7, -1, -2	(Forman et al. 2005)
Ti-6Al-4V alloy	0, 0.5, 0.7, -0.1, -1, -3, -5	(Zhang, Yang, and Lin 2015)
4340 Steel	0, 0.1, 0.5, 0.7, -1	(Sadananda and Vasudevan 2003)

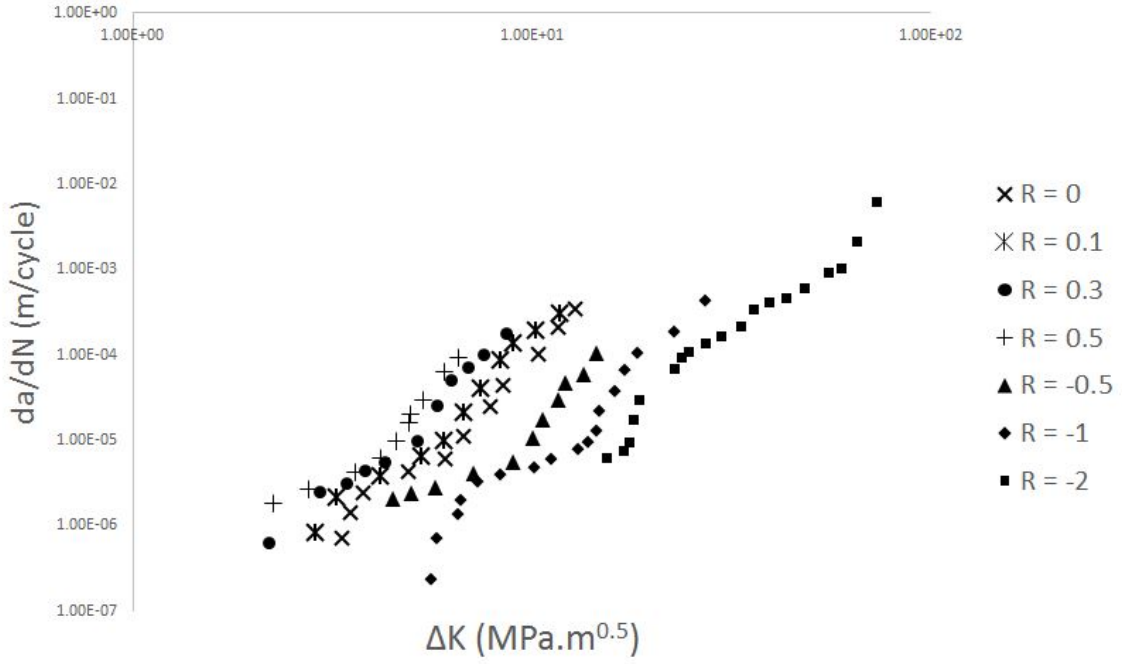

Figure 11. Constant amplitude loading test data of Al 2024 alloy

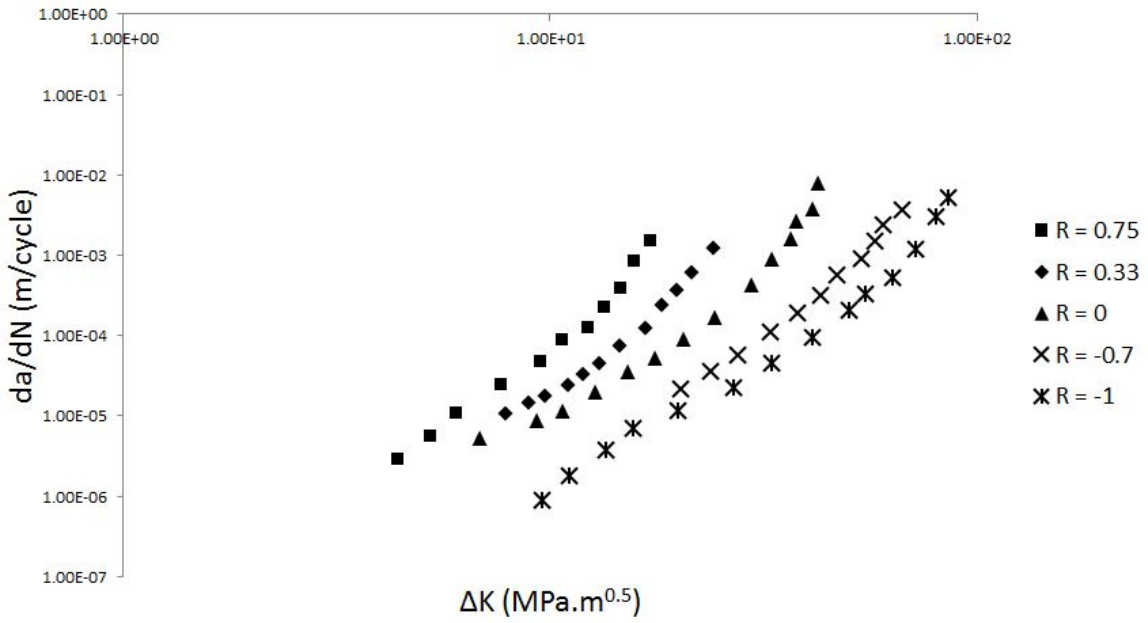

Figure 12. Constant amplitude loading test data of 7075-T6 Al alloy

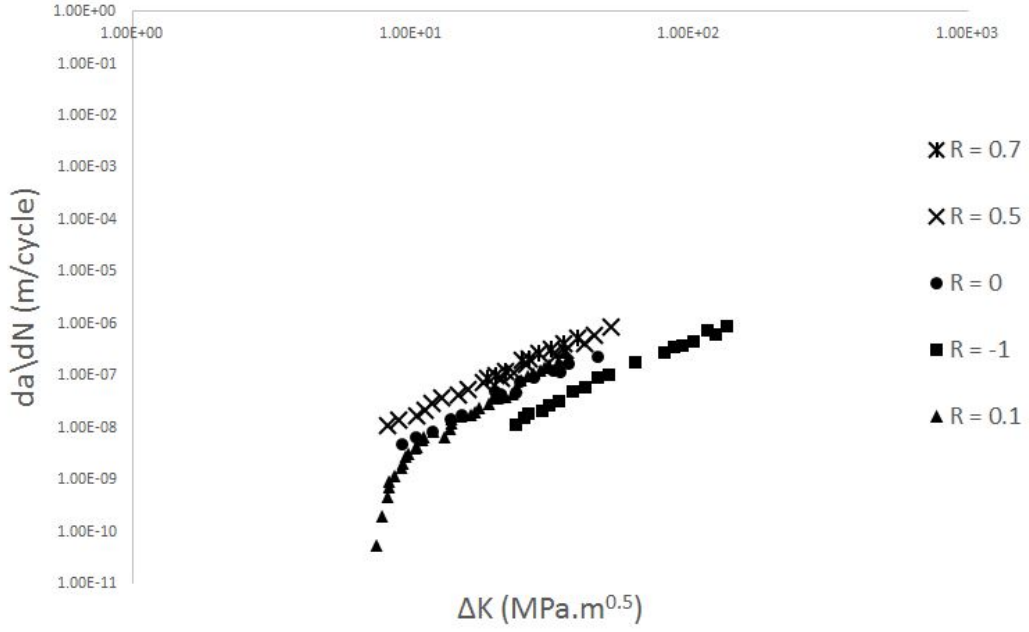

Figure 13. Constant amplitude loading test data of 4340 Steel

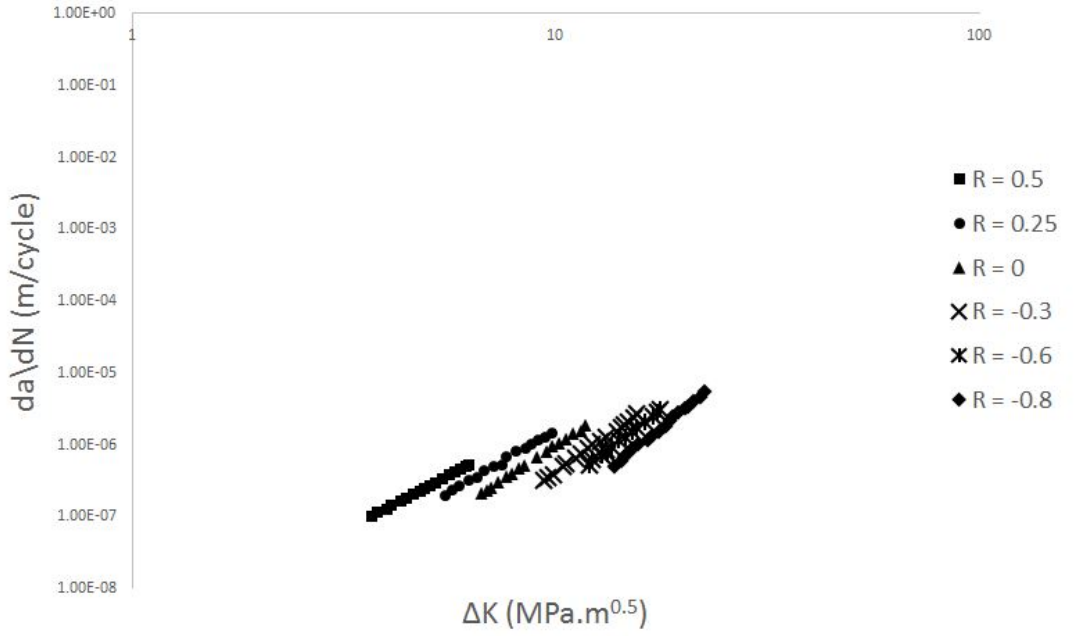

Figure 14. Constant amplitude loading test data of AM60B Mg alloy

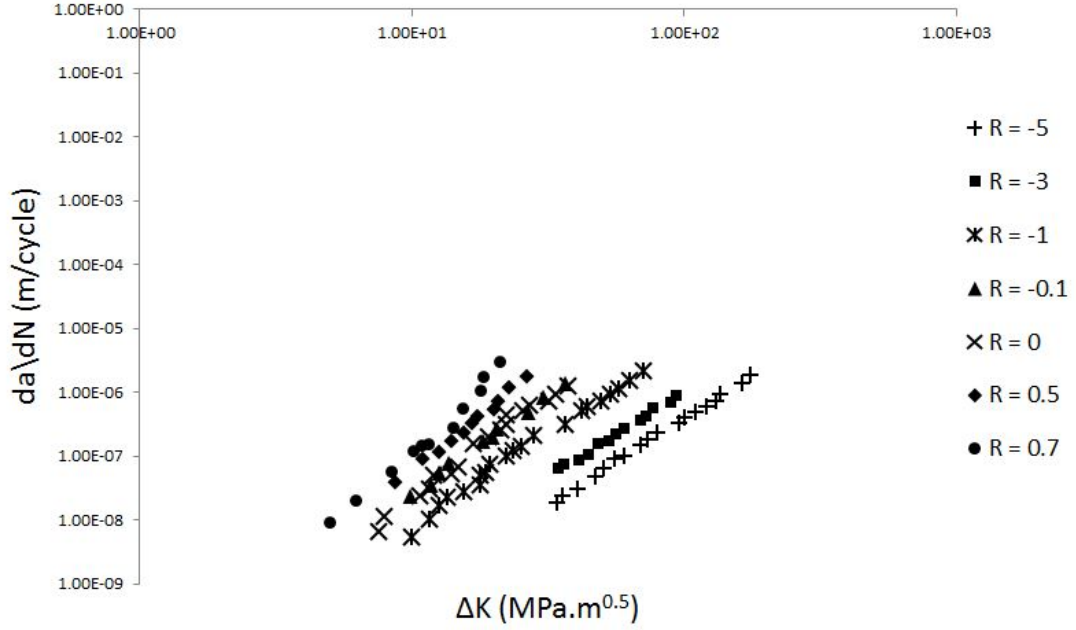

Figure 15. Constant amplitude loading test data of Ti-6Al-4V Titanium alloy

The fatigue crack growth data collapse into a single master curve for different load ratios, indicating that the crack closure can be used to explain the mean stress effect.

An equivalent stress intensity factor is used to collapse the test data into a single curve. Figure. 16 – 19 plots da/dN vs ΔK_{eqn} curves, for evaluating the ability of model for each material. The equivalent stress intensity factor ΔK_{eff} is given as

$$\Delta K_{eq} = \left(\frac{U\Delta K^{B+1}}{(1-R)^{B}}\right)^{0.5} \tag{2.21}$$

ΔK obtained from plots 11 to 15 and model parameter B obtained from Table 5 are used in the equation above to calculate ΔK_{eq} for each material and are plotted against model prediction for R = 0. The predictions show a good corelation with the experimental data as shown in the figure below.

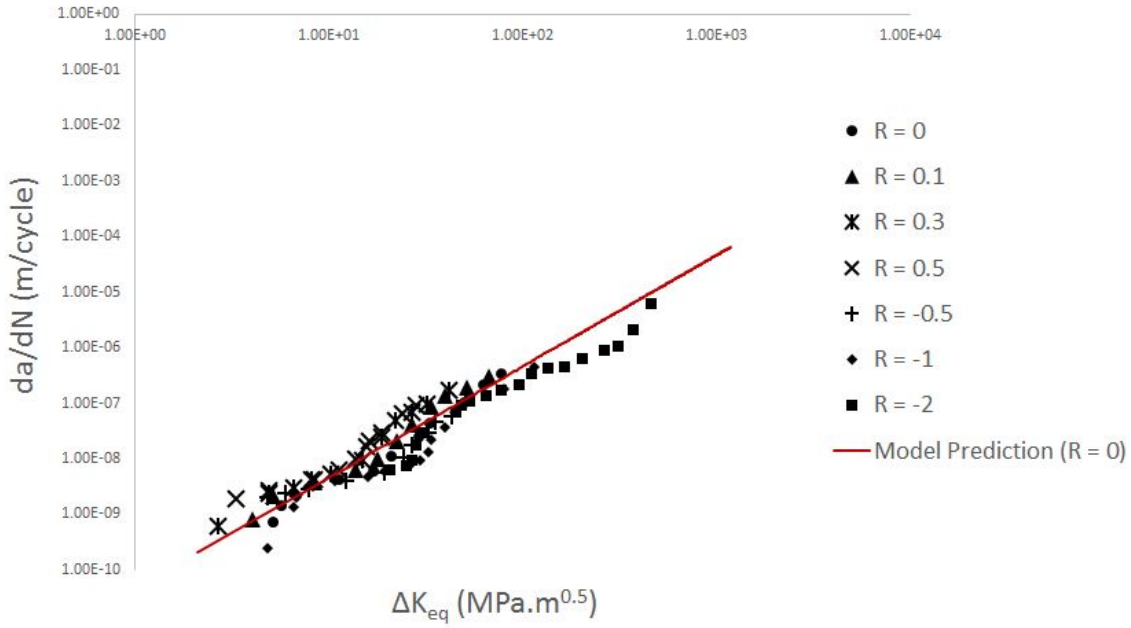

Figure 16. Comparison of model prediction with test data of Al2024 alloy as a function of ΔK_{eq}

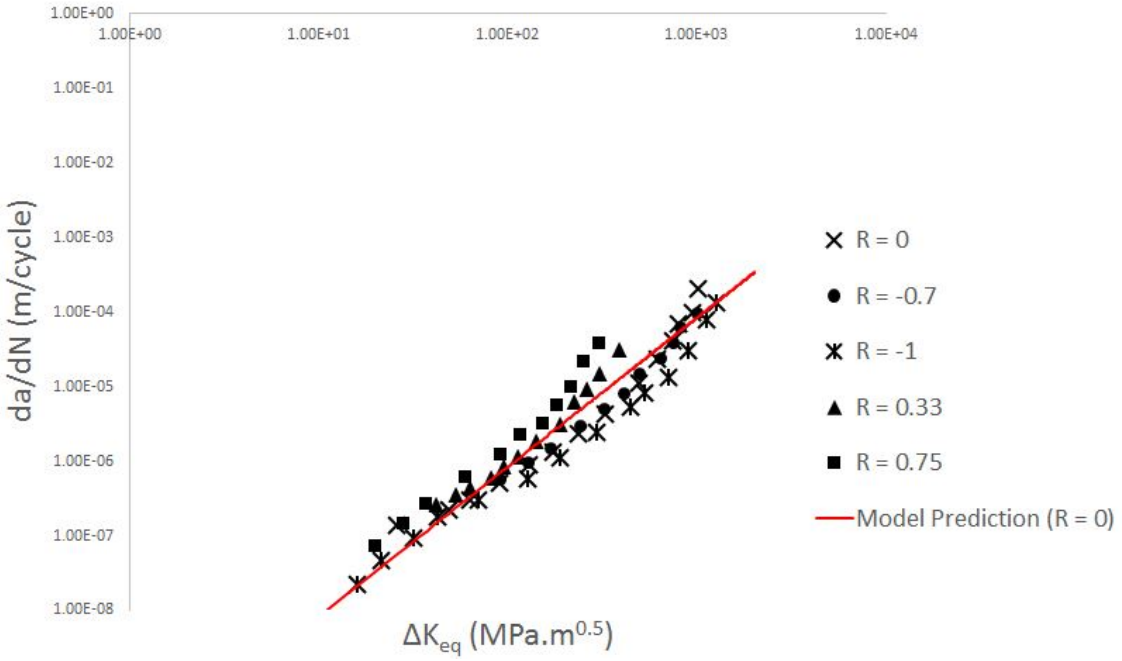

Figure 17. Comparison of model prediction with test data of Al7075-T6 alloy as a function of ΔK_{eq}

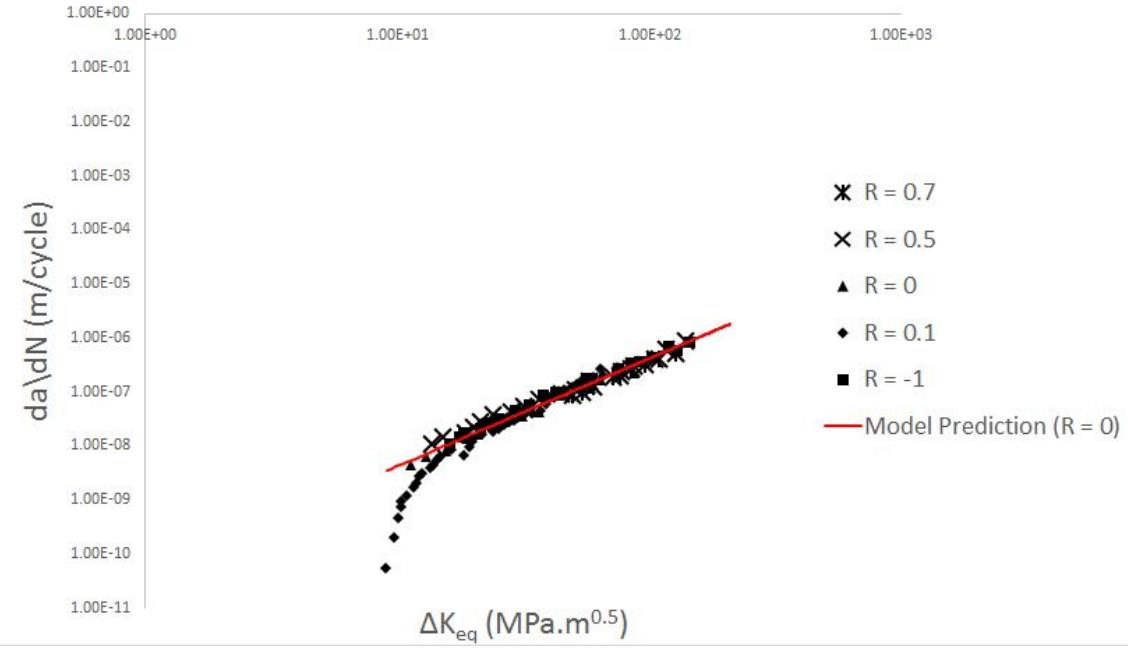

Figure 18. Comparison of model prediction with test data of 4340 Steel as a function of ΔK_{eq}

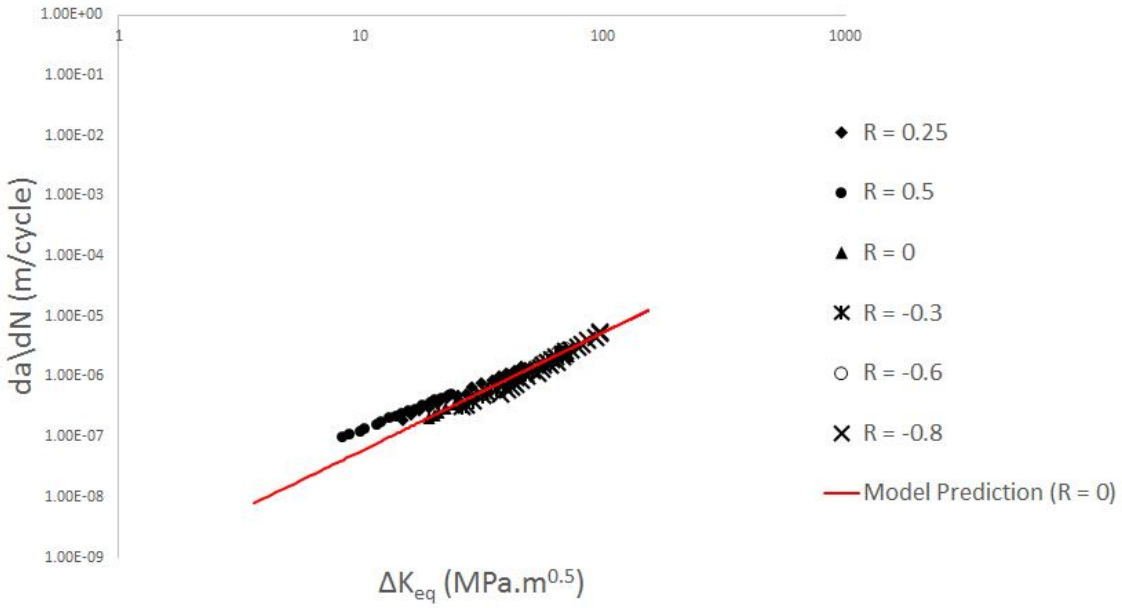

Figure 19. Comparison of model prediction with test data of AM60B Mg alloy as a function of ΔK_{eq}

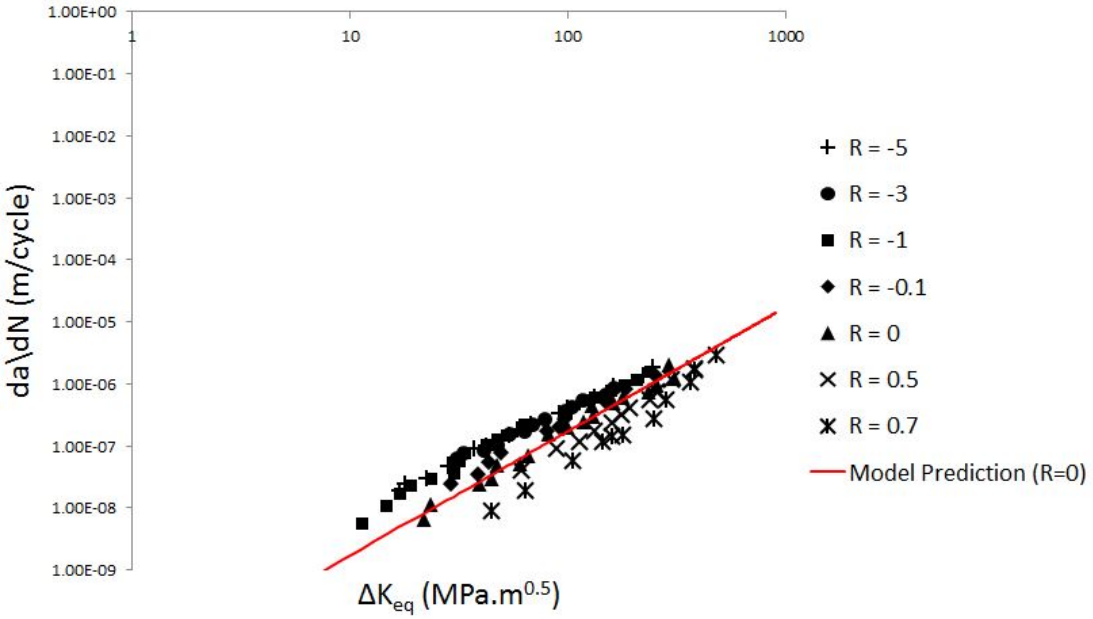

Figure 20. Comparison of model prediction with test data of Ti-6Al-4V alloy as a function of ΔK_{eq}

Chapter 3

FATIGUE CRACK GROWTH UNDER VARIABLE AMPLITUDE LOADING

3.1 Overview

Based on the improved small time scale model introduced in the previous chapter, the prediction results are in good agreement with the test data for a wide range of metallic materials under constant amplitude loading. However, most structures or industrial components in real life are subjected to complex loading spectrum. It brings the necessity to model fatigue crack growth rate under variable amplitude loading for design and life predictions. Several models has been proposed by researchers to predict and understand crack growth under variable loading. Most of the work has been done on single peak tensile overload which leads to crack growth retardation. Several other load scenarios have also been investigated by various researchers. The retardation and acceleration in crack growth rate due to overload, underload and overload followed by an underload has been investigated by Yen and Teheri (Yuen and Taheri 2006) and Rushton and Taheri (Rushton and Taheri 2003) and proposed few modifications to the Wheeler's model.

Various mechanisms have been proposed to explain fatigue crack growth under variable amplitude loading. As reviewed in the chapter 2, some of them are crack tip blunting, crack closure, hardening effect and residual stresses at the crack tip. Often these mechanisms operate simultaneously to affect the overall crack growth rate under variable amplitude loading. However, it is understood from the various research studies that plasticity induced crack closure have been considered the most

important fatigue crack growth mechanisms. In this chapter, the small time scale model is developed to predict under variable loading spectrum. Firstly, crack opening stress is modelled based on the largest monotonic and reversed plastic zone size in the load history. The model is modified to assume the maximum memory stress as a function of the current and overload plastic zone, and the current crack length. The retardation effect on crack growth due to an overload within a constant amplitude loading is investigated. The sensitivity of different materials to overload are explained to indicate that the size of the monotonic plastic zone is affected by an effective plastic zone co-efficient. Subsequently, a new parameter, referred to as sensitivity parameter is introduced to evaluate the affected zone size on different materials. The sensitivity parameter establishes an effective plastic zone radius is obtained with experimental data for different materials, and have no tangible physical meaning; as they have been developed by best fitting the test data to the closure equation, so that a better match to the retarded fatigue cycles could be obtained. Further more, crack closure due to load interaction effects is investigated. The integrity of the model combining the effects of overload and underload is validated. Several other block loadings are also used to validate the improved small time scale model.

3.2 Methodology Development

3.2.1 Crack Closure under Variable Amplitude Loading

Under cyclic loading, the stress field ahead of the crack tip is affected to form a larger monotonic plastic zone (Yang, Zhang, and Liu 2014) and a cyclic reversed plastic zone within the monotonic zone. This plastic deformation of the material

results in crack closure. Under constant amplitude loading, the crack opening is merely approximated to be constant. Based on this, a simple analytical crack closure solution was proposed in the previous chapter for both positive and negative stress ratios. Under variable amplitude loading, the crack opening stress is understood to change every cycle. For instance, application of an overload causes the crack opening stress to increase rapidly and gradually decrease to the steady state. This indicates the crack growth retardation. While an underload has the reverse effect and indicates crack growth acceleration. To account for the change of crack opening stress level, the virtual crack annealing method is once again used to model these effects. The value of the crack opening stress is not identical to that of the closure stress in the previous cycle. Under this hypothesis, the analytical approximation of crack opening stress can be obtained from Eq.

$$\frac{\pi}{8}\left(\frac{\sigma_{max}-\beta\sigma_{min}}{2\sigma_y}\right)^2\pi(a-d)-\frac{\pi}{8}\left(\frac{\sigma_{max}-\sigma_{cl}}{2\sigma_y}\right)^2\pi(a)=\frac{\pi}{8}\left(\frac{\sigma_{op}-\beta\sigma_{min}}{\sigma_y}\right)^2\pi(a-d) \quad (3.1)$$

The above equation based on virtual crack model can be rewritten using the monotonic zone size and the reversed plastic zone size in the load history as

$$\frac{\pi}{8}\left(\frac{\left(\frac{r_f}{\alpha\pi aY}\right)^{0.5}\sigma_y-\beta\sigma_{min}}{2\sigma_y}\right)^2\pi(a)-d_r=\frac{\pi}{8}\left(\frac{\sigma_{op}-\beta\sigma_{min}}{\sigma_y}\right)^2\pi(a) \quad (3.2)$$

where ρ_f and d_r are the monotonic plastic zone size and the reversed cyclic plastic zone size in the load history and are evaluated as

$$r_f=\alpha\left(\frac{K}{\sigma_y}\right)^2 \quad (3.3)$$

$$d_r=\frac{\pi}{8}\left(\frac{K_{max}-K_{cl}}{2\sigma_y}\right)^2 \quad (3.4)$$

The reversed plastic zone is estimated based on dugdale's model, however the co-efficient α to evaluate the monotonic plastic zone size is further investigated in the subsection 3.2.3. Finally, Eq.(3.2) is rewritten to solve for crack opening stress σ_{op} as

$$\sigma_{op} = \beta\sigma_{min} + ((\frac{(\frac{r_f}{\alpha\pi aY})^{0.5}\sigma_y - \beta\sigma_{min}}{2})^2 - \frac{8{\sigma_y}^2}{\pi^2 aY}d_r)^{0.5} \tag{3.5}$$

In the next subsection, the above equation is developed to predict crack opening stress under an application of single overload or underload.

3.2.2 Effect of Single Overload or Underload

It is well known that on the application of a tensile overload, the fatigue crack growth rate has been shown to retard. During a tensile overload, the magnitude of the residual compressive stress field ahead of the crack tip is large and increases the level of crack opening stress when the crack enters this compressive plastic region. The crack opening stress level increases instantaneously to the maximum value, and then gradually attains a steady state as the crack penetrates the large monotonic plastic zone in the subsequent cycles. To account for this retardation effect, the monotonic plastic zone size r_f under variable loading is expressed as a function of the current crack length and the overload plastic zone size r_{OL}.

As illustrated in Figure. 21 below, when the current monotonic plastic zone size reaches the large monotonic boundary, the crack opening stress returns to a steady state. If a_i and ρ_f are the current crack length and monotonic plastic zone size, and a_{OL} and ρ_{OL} are the overload crack length and monotonic plastic zone size, the following relationship can be established.

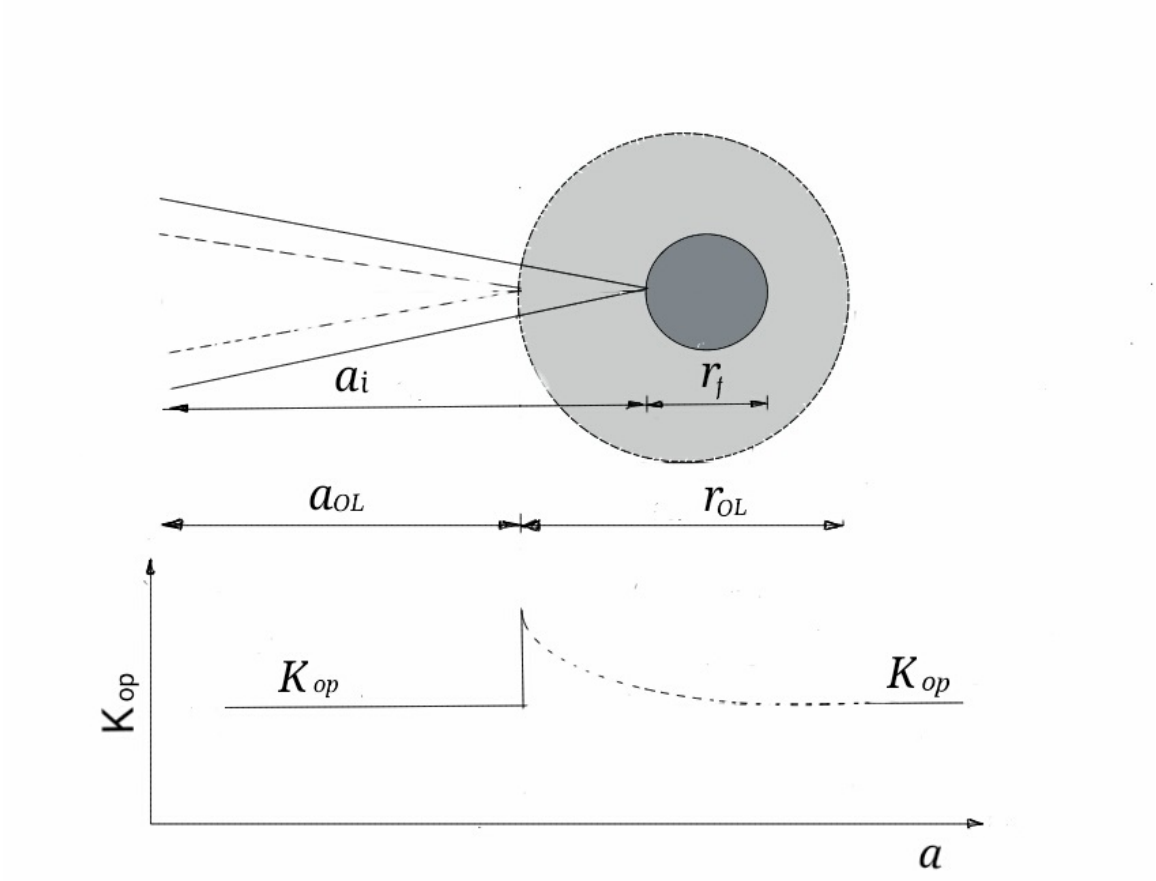

Figure 21. A schematic representation of crack opening stress σ_{op} under load sequence with single overload

$$|r_f + a_i = a_{OL} + r_{OL}, |\, r_f = a_{OL} + r_{OL} - a_i \tag{3.6}$$

The large monotonic compressive plastic zone is evaluated as

$$r_{OL} = \alpha(\frac{K_{OL}}{\sigma_y})^2 \tag{3.7}$$

On the contrary, when an underload is applied in the constant amplitude baseline loading, the residual stress field ahead of the crack tip is tensile. As illustrated in Figure 22, an enlarged cyclic plastic zone embeds over the constant amplitude reversed plastic zone (RL 1998). The crack propagation rate will not resume the steady state

characteristics unless the crack propagates through the enlarged cyclic plastic zone. This causes the crack opening stress level to decrease and accelerate the fatigue crack growth rate. This mechanism is modelled by depleting the cyclic plastic zone with respect to largest cyclic plastic zone in the load history $d_{r,max}$.

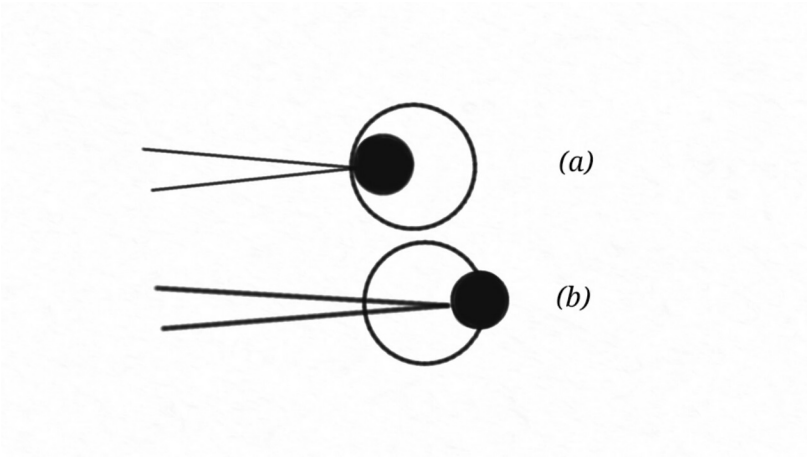

Figure 22. Cyclic plastic zone: (a) immediately after a compressive underload, (b) the crack propagating through the underload plastic zone.

The retardation effect due to enlarged plastic zone is modelled by substituting Eq.(3.6) into Eq.(3.5). The acceleration in crack growth and decrease in opening stress level is modelled by rewriting the σ_{min} as σ_{minmem} in Eq.(3.5). The final form of the equation to calculate opening stress is given as

$$\sigma_{op} = \beta\sigma_{minmem} + \left(\left(\frac{\left(\frac{a_{OL}+r_{OL}-a_i}{\alpha\pi aY}\right)^{0.5}\sigma_y - \beta\sigma_{minmem}}{2} \right)^2 - \frac{8{\sigma_y}^2}{\pi^2 aY}(d_{r,max} - a_i) \right)^{0.5} \quad (3.8)$$

3.2.3 Modified Plastic Zone Size Co-efficient

The plastic zone size is usually related to the stress intensity factor K and material yield strength σ_y, by the coefficient α. Several approaches has been proposed by

various researchers to establish α. Some obtained by considering linear elastic material behavior, while others are obtained considering perfectly plastic material behavior. In the previously proposed model based on Eq.(3.8), the affected monotonic plastic zone size based on dugdale's model is approximated to be

$$r_f = \frac{\pi}{8}(\frac{K}{\sigma_y})^2 \tag{3.9}$$

Using the above relation for plastic zone size with $\alpha = \frac{\pi}{8}$, the small time scale model predicted lesser life cycles compared to that of the test date for different materials. This signifies that the demonstrated affected zone size does not match the actual zone size. Moreover, it is understood that for different materials, the actual affected zone would be different than that demonstrated by the model. Therefore it could be concluded that the materials sensitivity to overload cycles varies from one material to another. In our investigation, a modification parameter γ is introduced to address the sensitivity of the material to an overload in an effective way.

In order to evaluate the sensitivity parameter γ, a portion of the overload plastic zone is considered in the Eq.(3.8). In other words, the crack opening stress is modified to account for the material's sensitivity to overload, described by the equation below

$$\sigma_{op} = \beta\sigma_{minmem} + \left((\frac{8(\frac{a_{OL}+\gamma r_{OL}-a_i}{\gamma\pi^2 aY})^{0.5}\sigma_y - \beta\sigma_{minmem}}{2})^2 - \frac{8{\sigma_y}^2}{\pi^2 aY}(d_{r,max} - a_i) \right)^{0.5} \tag{3.10}$$

Comparing equations (3.8) and (3.10) reveals that an additional parameter is included in the original crack opening stress based on virtual crack method. This parameter accounts for material's sensitivity to an applied overload. This sensitivity factor acts over the crack length until the current plastic zone reaches the large monotonic boundary. The parameter γ are determined based on the experimental

data obtained for different materials with various overload ratios, as presented in Table.

Table 7. Sensitivity parameter γ for different materials

Material	γ	OL ratios
AM60B	1.3	1.75, 2.0
Al 2024-T3	4.54	2.0
D16 Al alloy	4	2.0
Al 7075-T6	3.33	2.0
Ti-6Al-4V	1.87	2.0

The figure illustrating the model predictions in case of an applied single overload, with the established sensitivity parameter γ is shown in section 3.3 under validation. Using the modified plastic zone size coefficient for various materials, the model is extended to predict growth rate under load interactions with the combined effect of overload and underload.

3.2.4 Overload-Underload Interactions

The modified crack opening stress model introduced in the previous section has the capacity of modelling crack growth retardation or acceleration due to an application of tensile single or multiple overloads or underloads in a constant amplitude baseline. However, the model is incapable of considering the combination of an overload and underload. Based on the state of art, when an underload is applied prior to an an overload, the change in the amount of retardation is assumed to be negligible (Murthy, Palani, and N. Iyer 2004). However, when an underload is applied followed by an overload, it has been observed that the retardation effect is lesser (Murthy, Palani, and N. R. Iyer 2007), indicating that a portion of the large monotonic plastic zone gets

depleted by the underload. To account for this effect, the plastic zone size increment caused by the underload is subtracted from the monotonic large boundary due to the overload. A schematic representation of the depletion in monotonic plastic zone size is illustrated in Figure23.

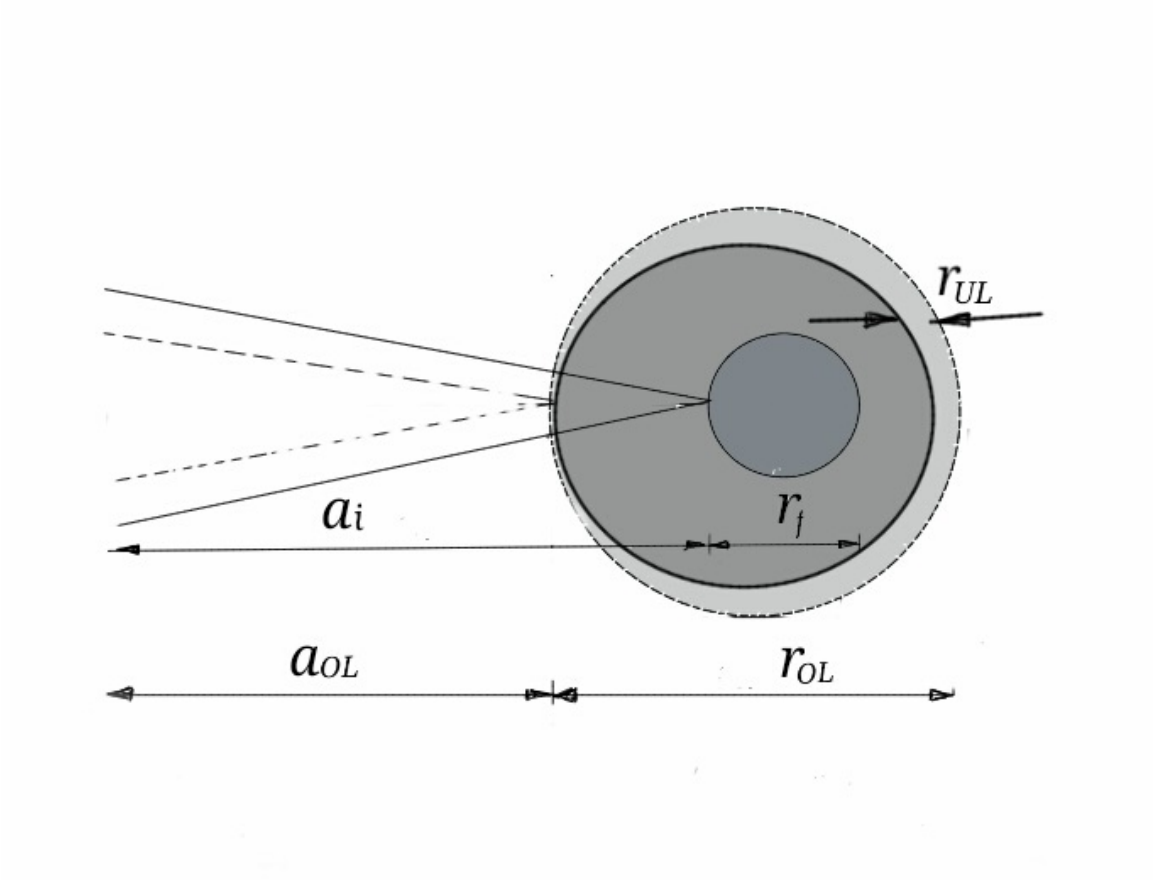

Figure 23. Schematic representation of depleting plastic zone sizes to account for the effect of underload following overloading (Huang, Torgeir, and Cui 2008)

The plastic zone size increment due to underload is understood to vary for different materials and is assumed that it can be addressed by the material sensitivity parameter γ as well. Under this hypothesis, Eq.(3.10) is rewritten to model the depleted large monotonic boundary

$$\sigma_{op} = \beta\sigma_{minmem} + \left(\left(4\left(\frac{a_{OL} + \gamma(r_{OL} - r_{UL}) - a_i}{\gamma\pi^2 aY}\right)^{0.5} \sigma_y - \frac{\beta\sigma_{minmem}}{2} \right)^2 - \frac{8{\sigma_y}^2}{\pi^2 aY}(d_{r,max} - a_i) \right)^{0.5} \tag{3.11}$$

where r_{UL} is monotonic tensile plastic zone size caused by the application of an underload, and can be calculated as

$$r_{UL} = \frac{\pi}{8}\left(\frac{(K_{min} - K_{minmem}}{\sigma_y}\right)^2 \tag{3.12}$$

The equation (3.11) for crack opening stress has the capacity to model growth rate under single or multiple overloads, underloads or the interaction of the two load types. A qualitative analysis to investigate the performance of the improved model is carried out and discussed in the next section.

3.3 Discussion

In this section, the capacity of the improved small time scale model is investigated by performing a qualitative analysis. As illustrated in Figure. 24 and 25, the effects of the sensitivity parameter γ and overload ratio (OLR) on predicted results when a single overload is applied can be explained. Based on Figure 24, the level of fatigue crack growth rate retardation will be changed with the sensitivity parameter, and the retardation phenomenon can be adequately simulated by fitting a relevant value for different materials. It is also understood that the crack growth retardation will be more with the increase in overload ratio. This can be clearly observed in Figure.25.

Moreover, to verify the simulation capability of the model under different loading sequences, Figure 26 describes five basic types of loading and Figure 27 depicts the

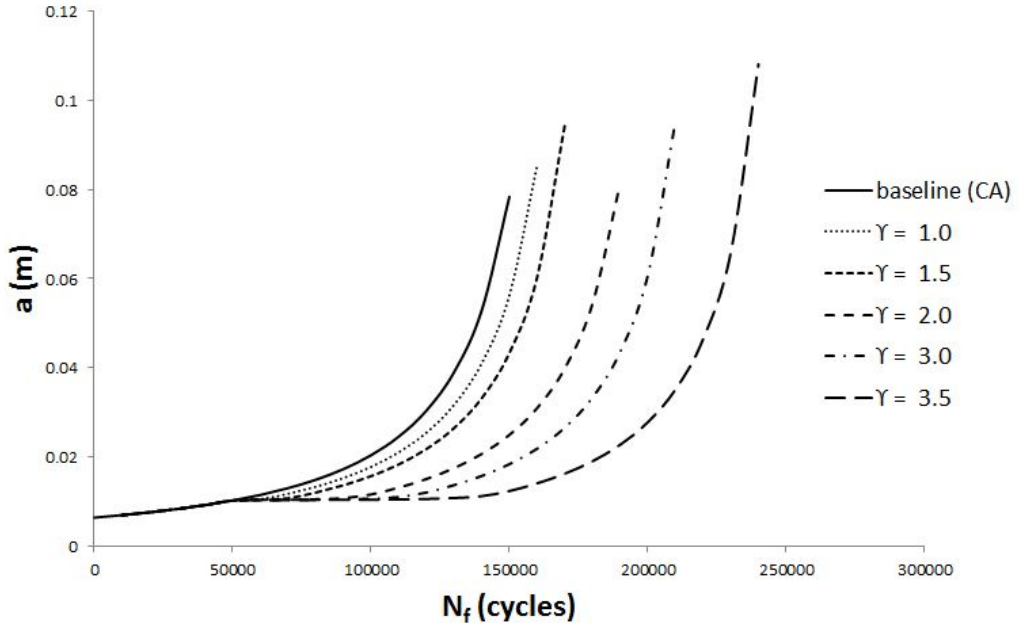

Figure 24. The effect of Sensitivity parameter γ on the predicted results

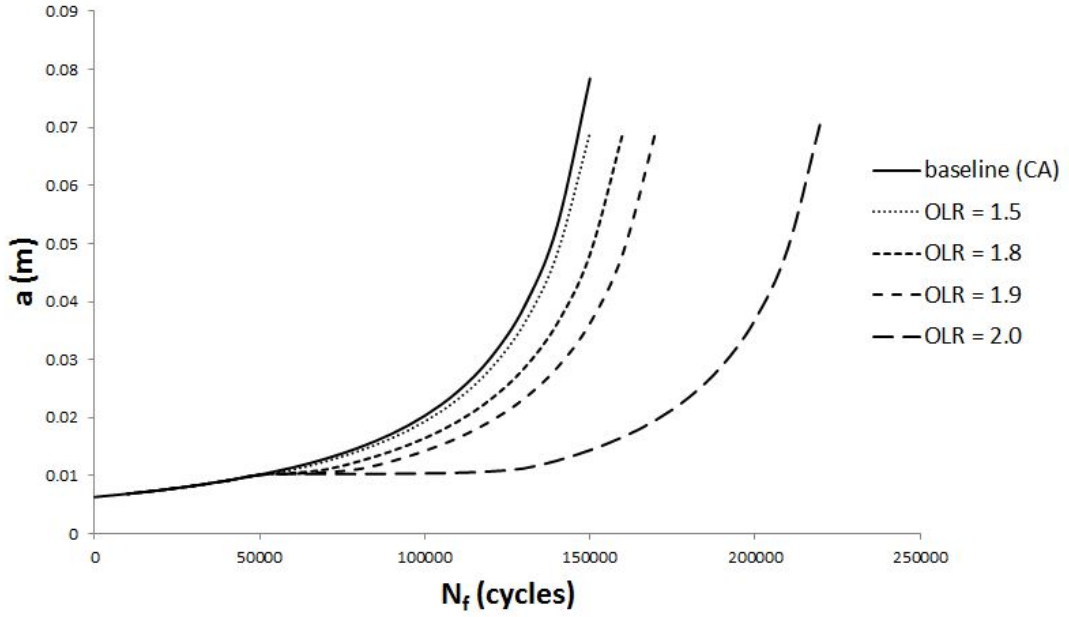

Figure 25. The effect of overload ratio R_{OL} on the predicted results

prediction curves of crack length (a) versus number of life cycles N_f under different load types. Different tendency of $a - N_f$ curves has been observed for the different

typed of loading mode. The fatigue life of the constant amplitude case is larger than the fatigue life of the case due to an underload, while the fatigue life is quite longer under a single applied overload. It can also be clearly observed that the fatigue life of the case (underload followed by overload) is shorter than that of just the overload. The simulated results are in accordance with the general agreements that are observed in the test data.

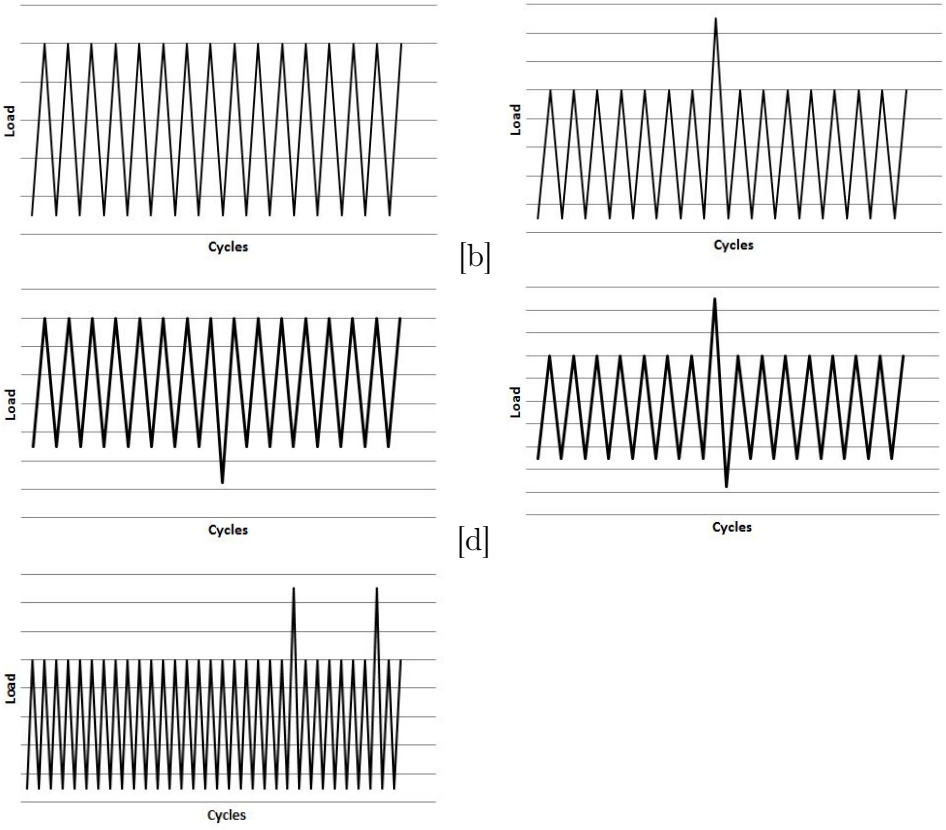

Figure 26. Basic loading modes

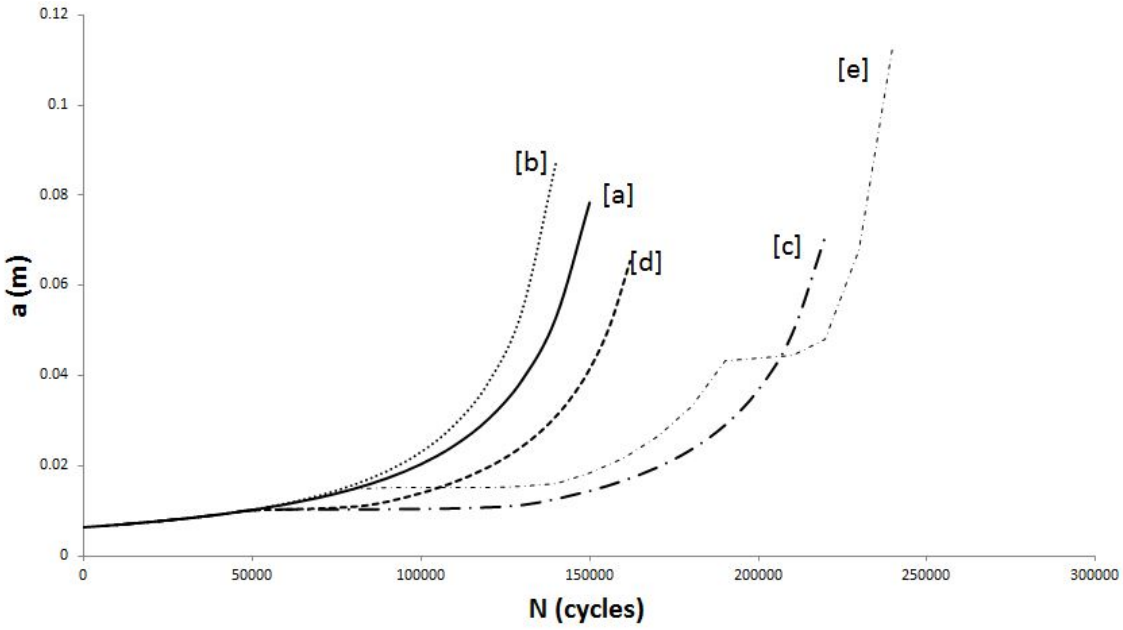

Figure 27. Predicted a-N curve for the basic loading modes mentioned above

3.4 Model Validation

In the previous section, the capacity of explaining the load interaction effects has been investigated by the qualitative analysis. In this section, the applicability of the small time scale model is further validated under variable amplitude loading (VAL) by comparing the predicted results with the fatigue crack growth experimental data. Several types of loading are considered including single and multiple spike tensile overloads, underloads, combination of overload and underload and variable sized block loading.

3.4.1 Single Spike Loading

In this section, test data for fatigue crack growth under a constant amplitude loading with single spike overload is used to fit the model parameter γ discussed in the section 3.2. In case of single overload, the overload ratio R_{OL} is given as σ_{OL}/σ_{max}. While in case of an underload, the underload ratio R_{UL} is defined as σ_{UL}/σ_{min}. A summary of all the test data collected for the single spike overload or underload case for the corresponding material and the references for each one of them are presented in the Table 8.

Table 8. Constant amplitude loading with single overload or underload

Load specs(Stress ratio)	Material	σ_{max}	References
CA(0.1) + OL(2)	AM60B	45 MPa	(Mehrzadi 2013)
CA(0.1) + OL(1.75)	AM60B	45 MPa	(Mehrzadi 2013)
CA(0.05) + OL(2)	7075-T6	68 MPa	(Zhao, Zhang, and Jiang 2008)
CA(0) + OL(2)	2024-T3	100 MPa	(Newman Jr 1997)
CA(0) + OL(2) + UL(-0.8)	2024-T3	100 MPa	(Newman Jr 1997)
CA(0.1) + OL(2)	Ti-6Al-4V	25 MPa	(Belnoue et al. 2010)
CA(0.1) + OL(2)	Ti-6Al-4V	20 MPa	(Belnoue et al. 2010)

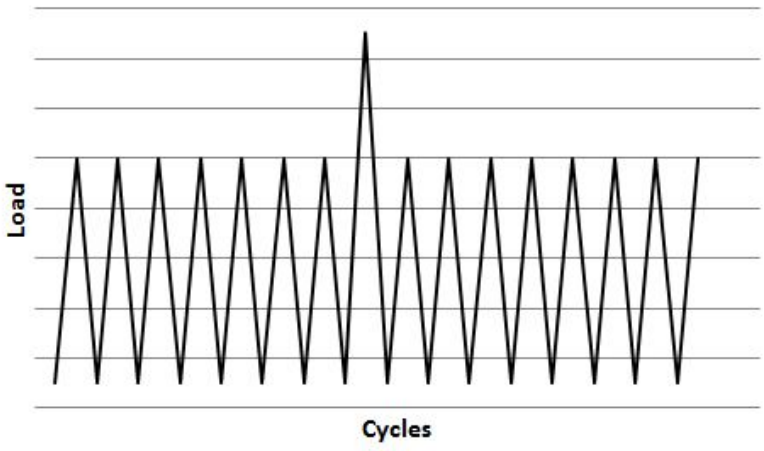

Figure 28. Constant amplitude baseline spectrum with single spike overload

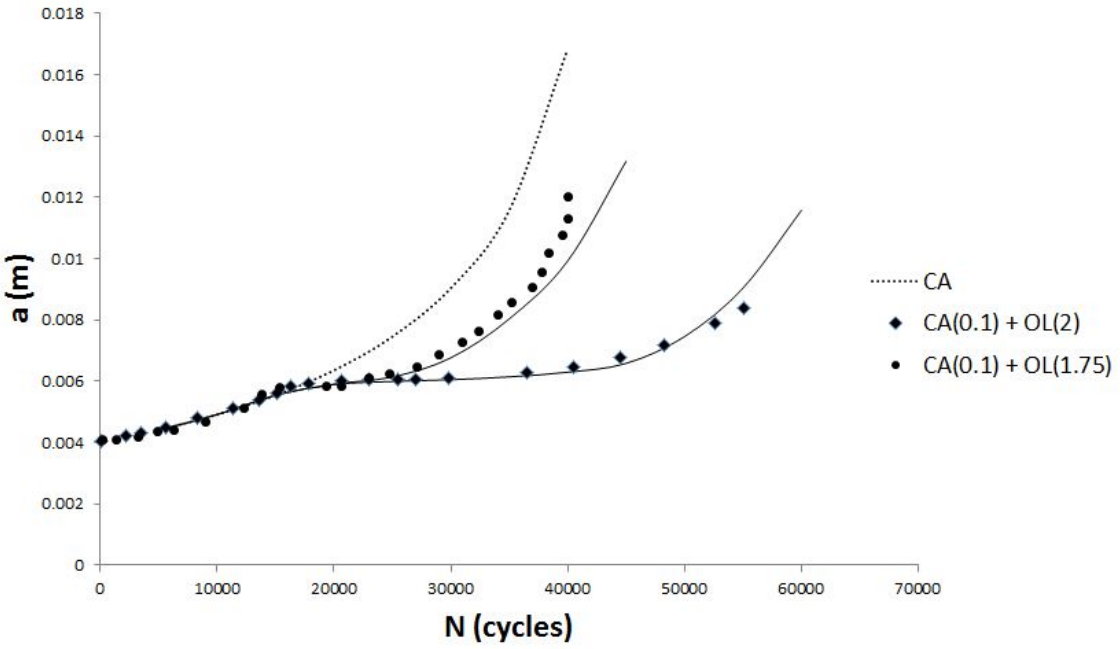

Figure 29. Comparison of predictions with test data of AM60B Mg Alloy under single overload

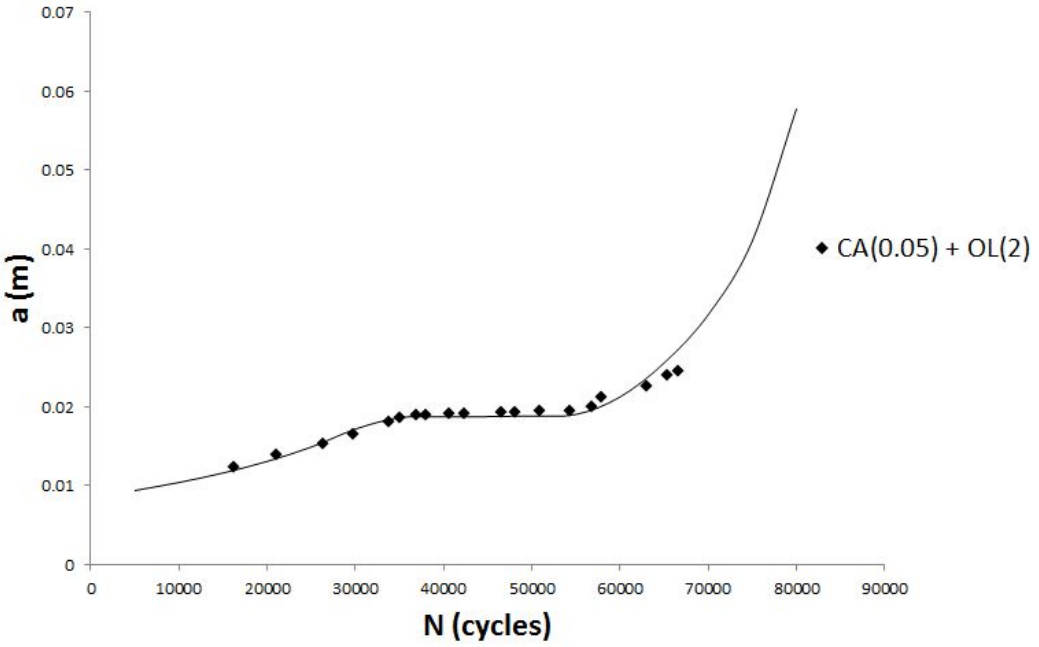

Figure 30. Comparison of predictions with test data of 7075-T6 Aluminum alloy under single overload

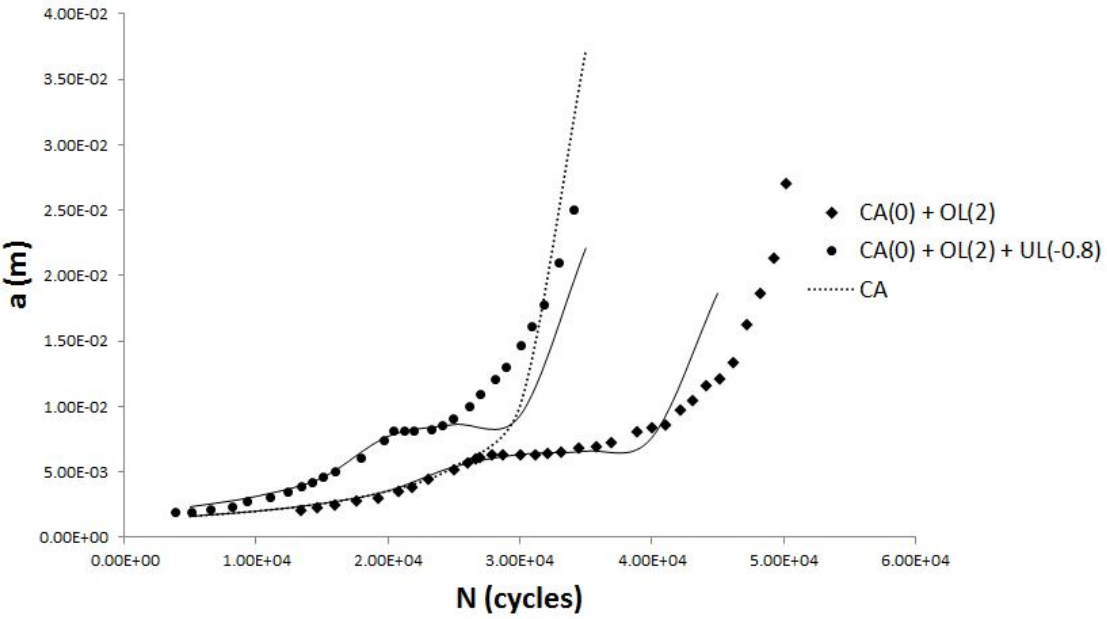

Figure 31. Comparison of predictions with test data of 2024 Aluminum alloy under single overload

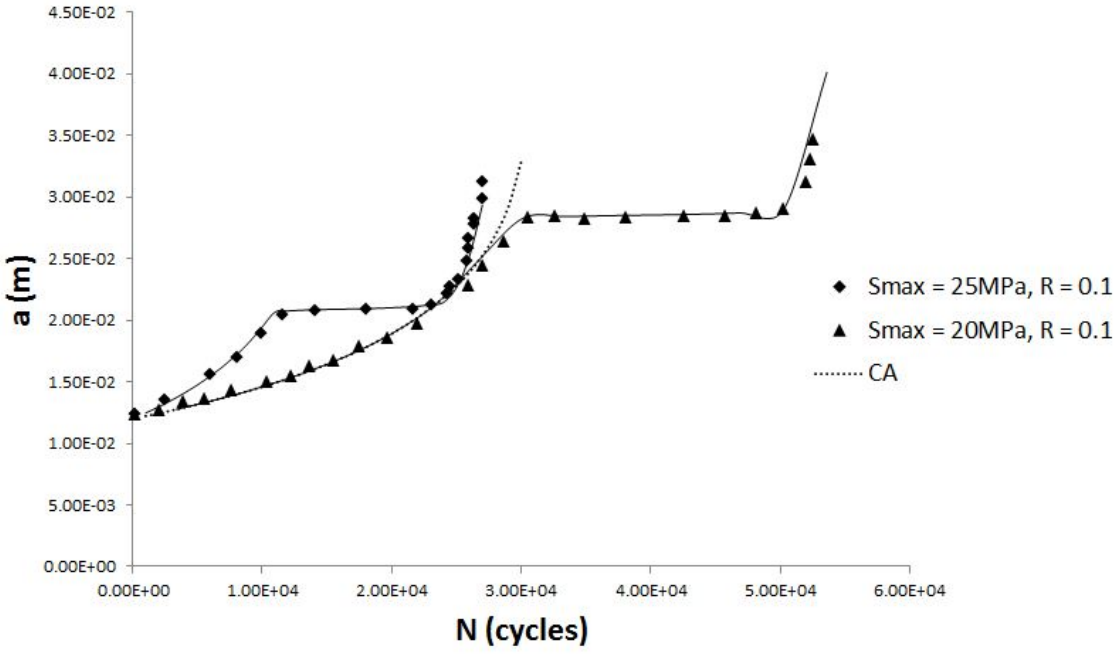

Figure 32. Comparison of predictions with test data of $Ti-6Al-4V$ Titanium alloy under single overload

3.4.2 Repeated Spike Loading

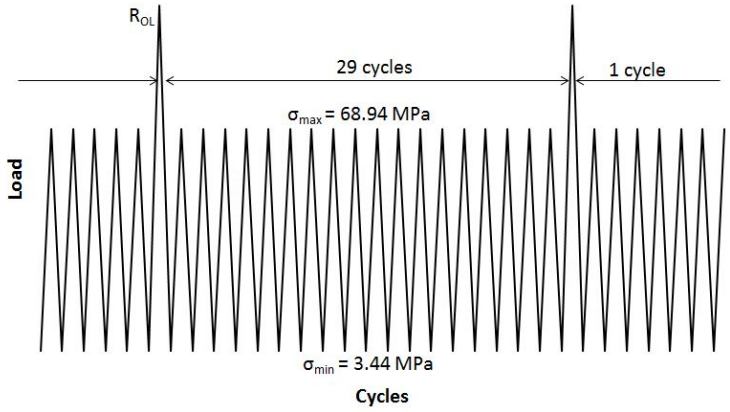

Figure 33. Constant amplitude load spectrum with repeated spike overload provided for test data of 7075-T6 alloy (Porter 1972)

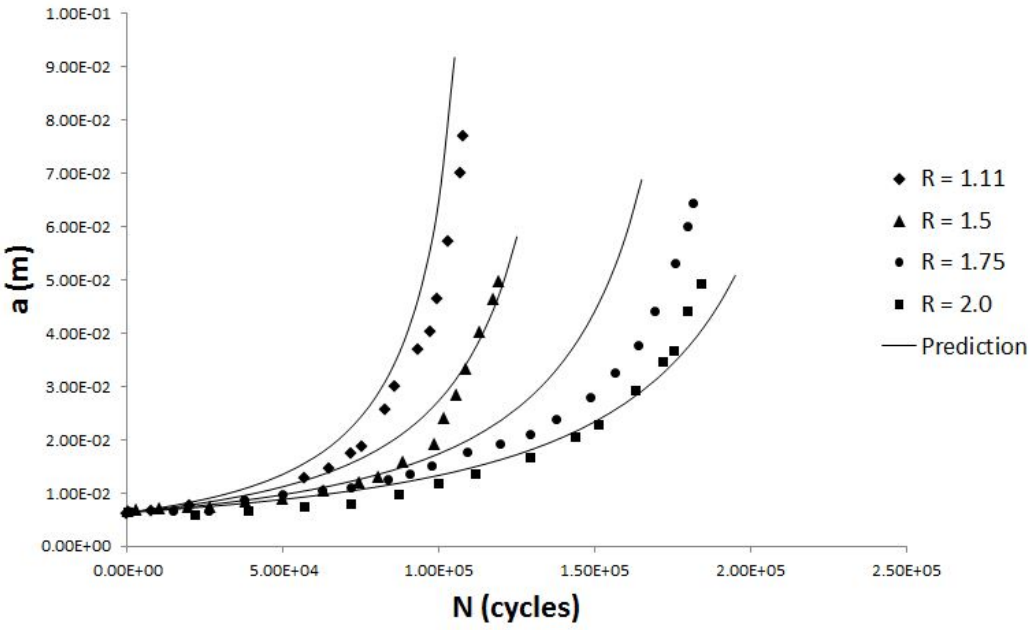

Figure 34. Comparison of predictions with test data of Al7075-T6 under repeated overloads with variable overload stress ratios

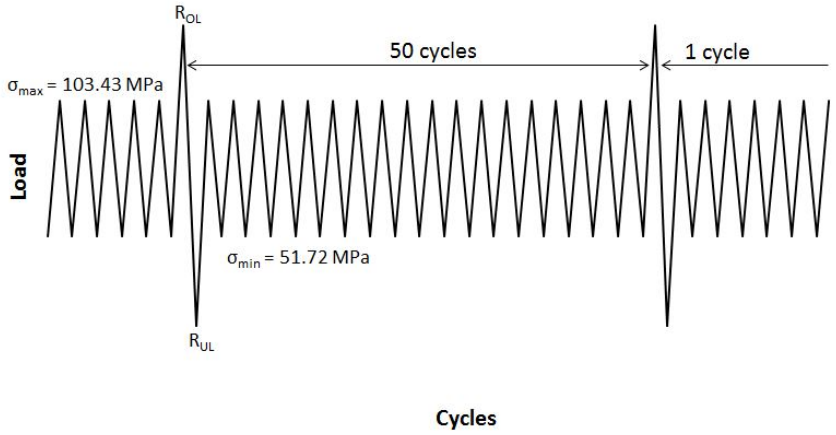

Figure 35. Constant amplitude load spectrum with repeated spike overload-underload provided for test data of 7075-T6 alloy (Porter 1972)

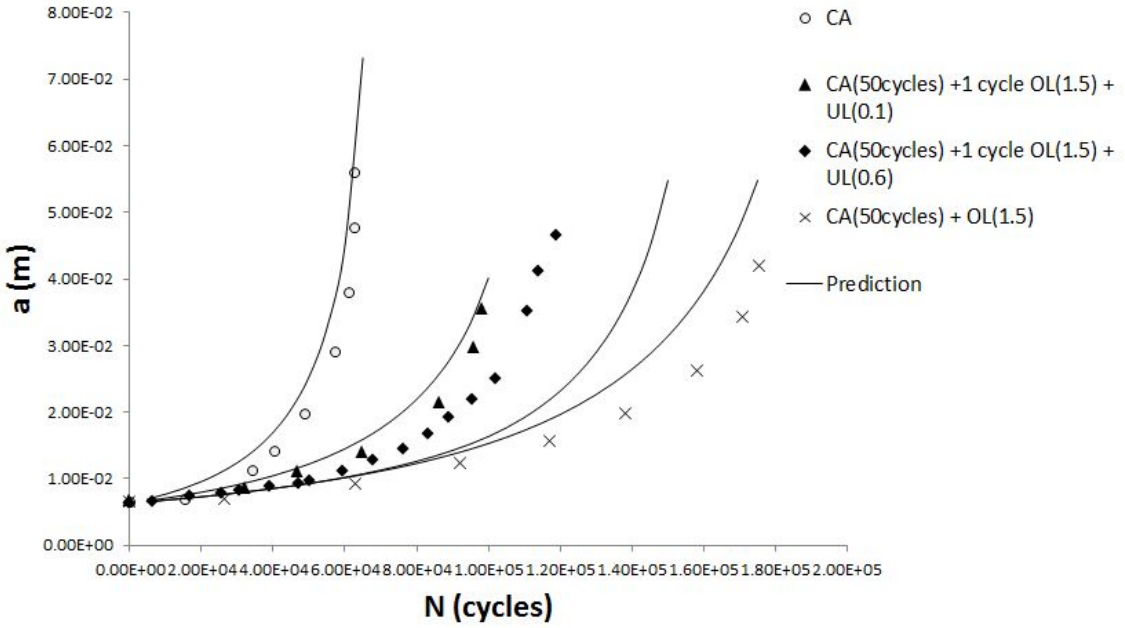

Figure 36. Comparison of predictions with test data of Al7075-T6 under repeated overload-underload

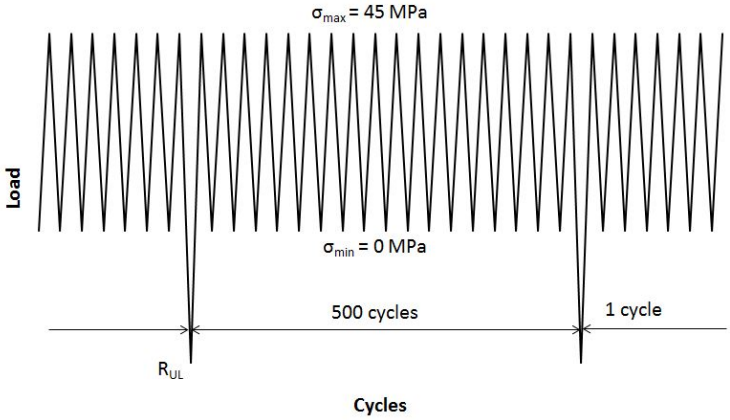

Figure 37. Constant amplitude load spectrum with repeated spike underload provided for test data of AM60B alloy (Mehrzadi and Taheri 2013)

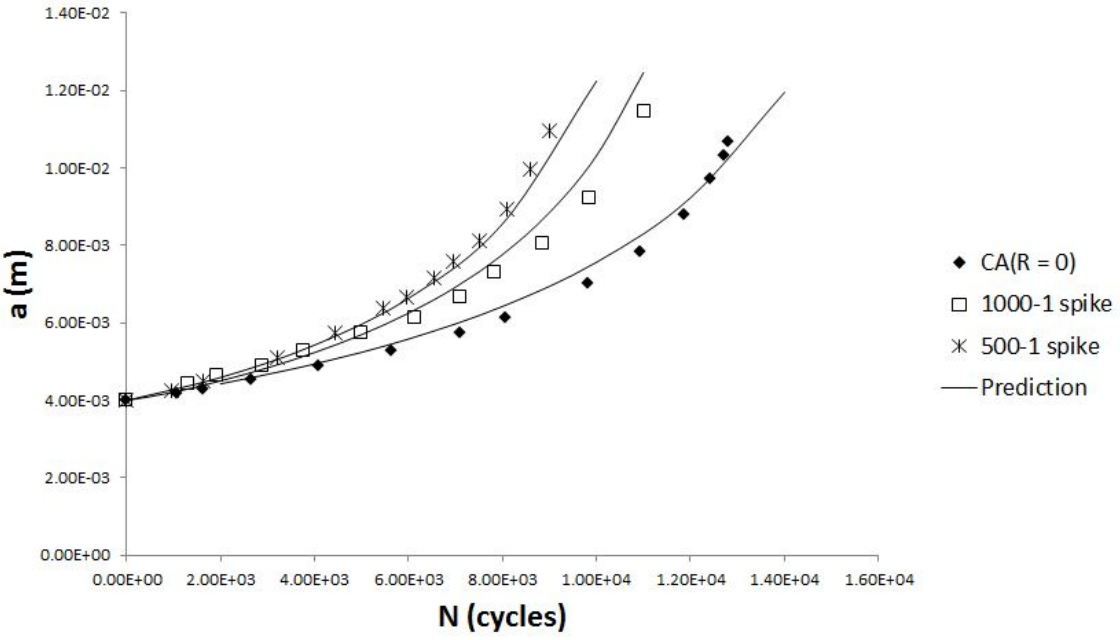

Figure 38. Comparison of predictions with test data of AM60B Mg alloy under repeated compressive spike underload

3.4.3 Variable Size Block Loading

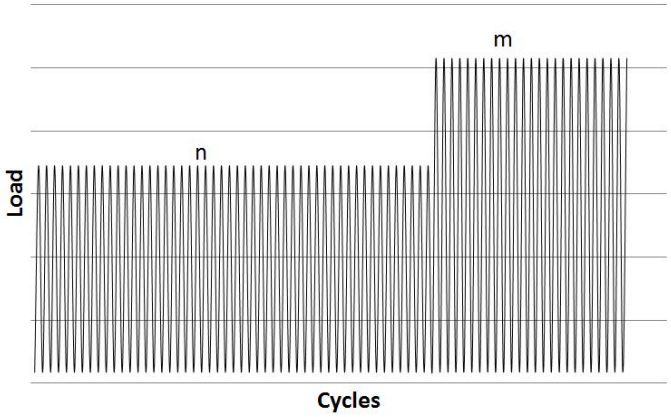

Figure 39. Variable size block load spectrum provided for test data for 7075-T6 (Porter 1972)

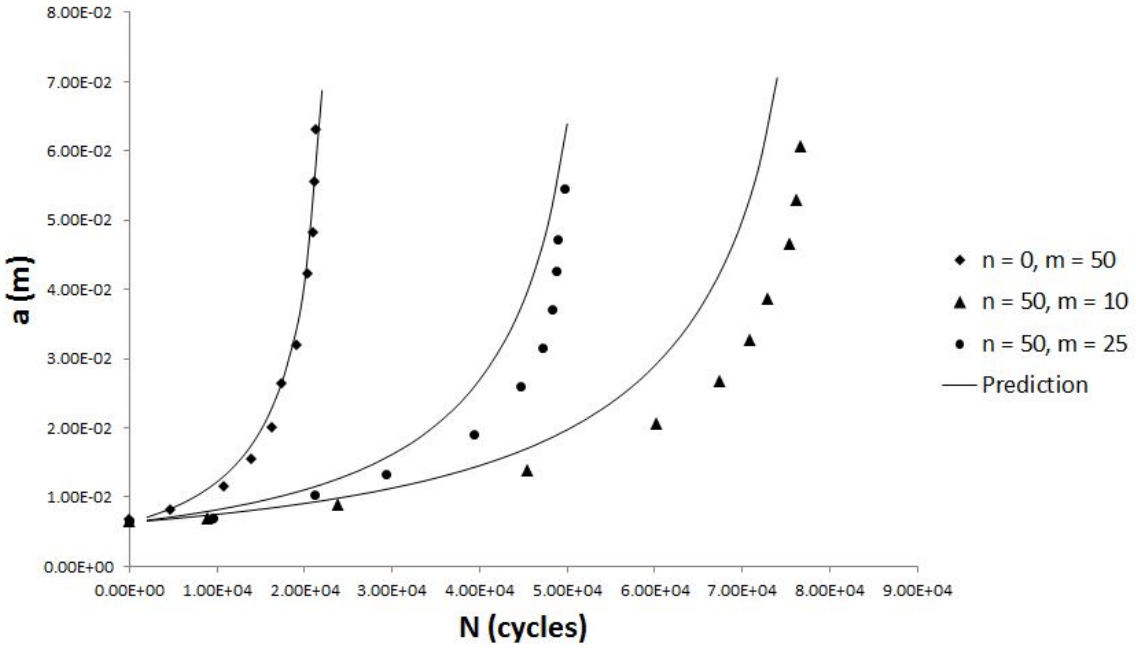

Figure 40. Comparison of predictions with test data of Al7075-T6 alloy under variable size block loading

3.4.4 Variable Spectrum Loading

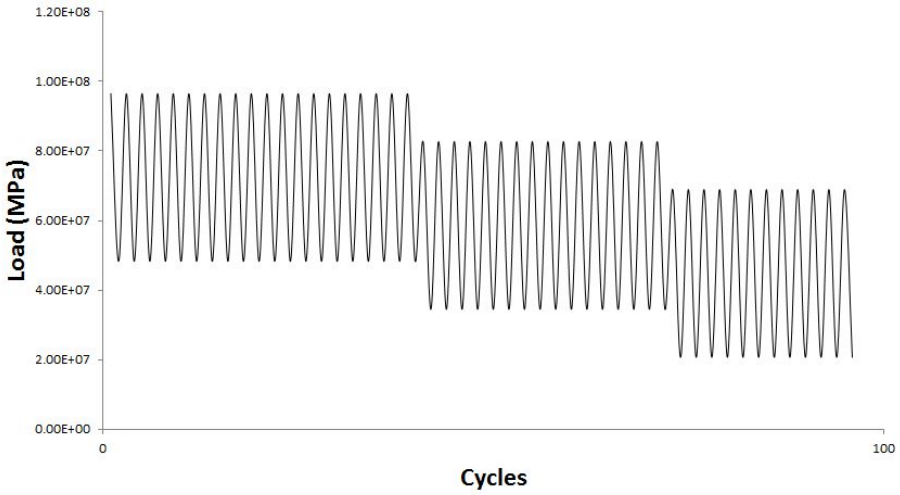

Figure 41. Loading spectrum P1 (Ray and Patankar 2001)

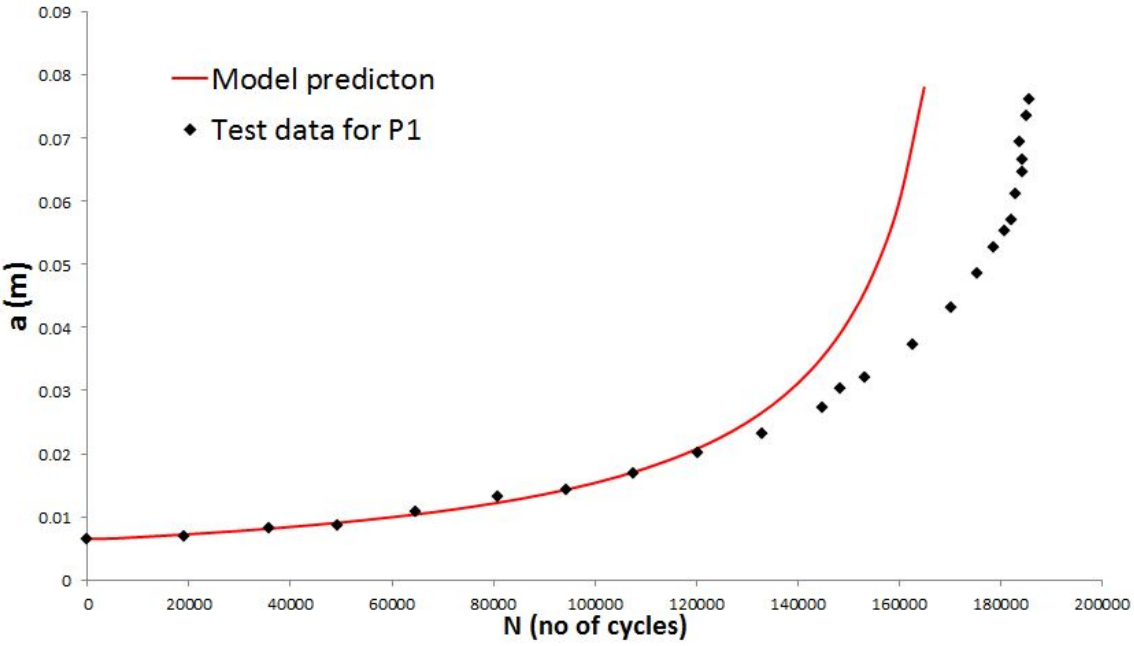

Figure 42. Comparison of predicted results with the test data of Al2024-T3

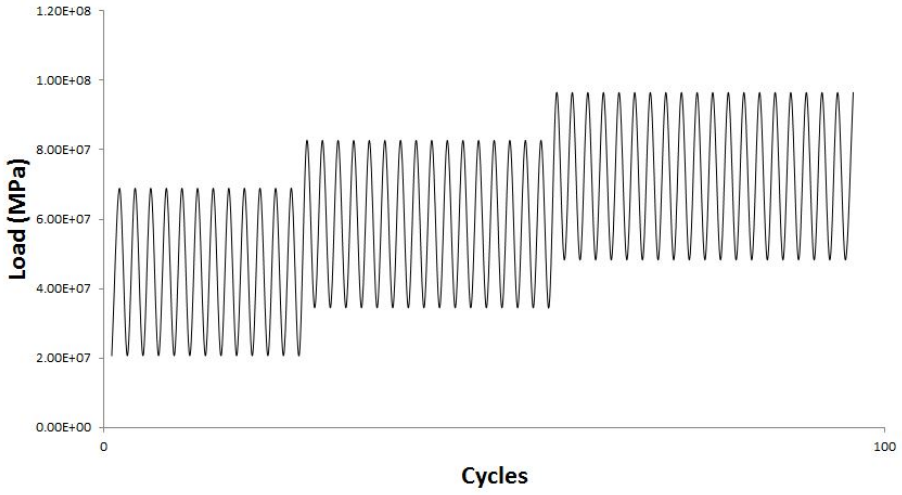

Figure 43. Loading spectrum P2 (Ray and Patankar 2001)

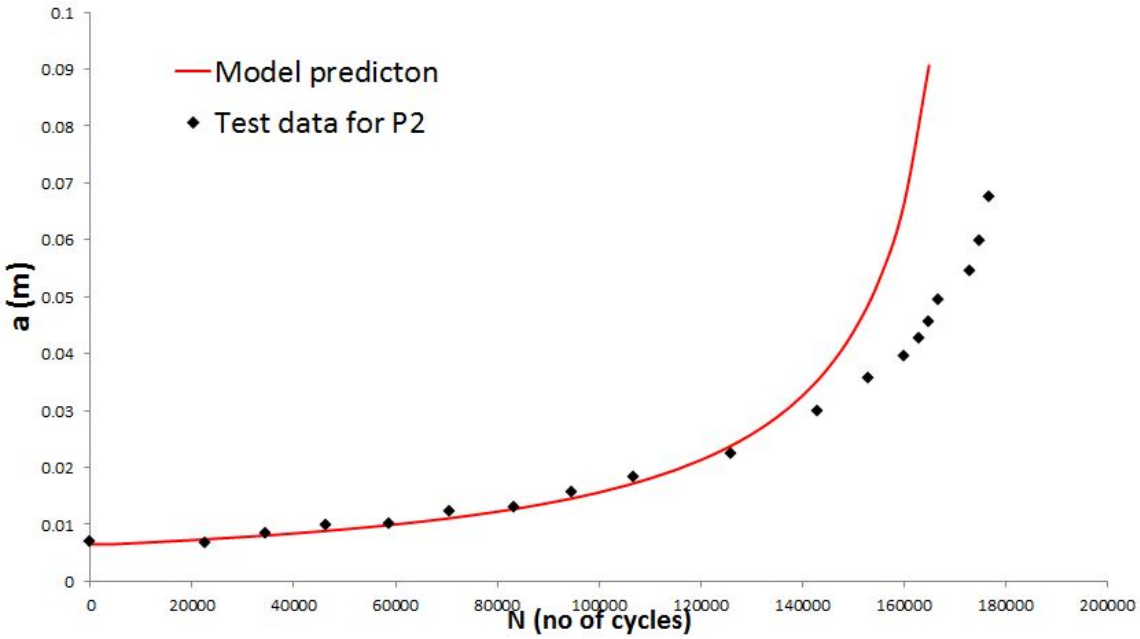

Figure 44. Comparison of predicted results with the test data of Al2024-T3

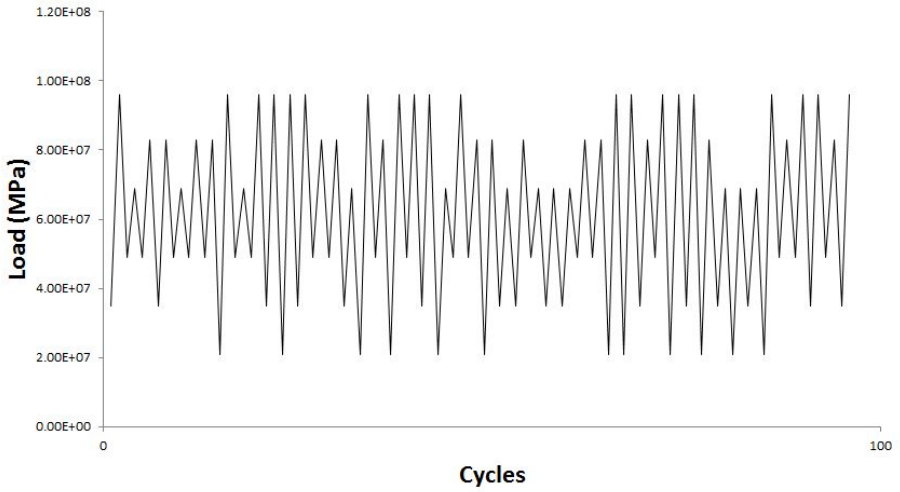

Figure 45. Loading spectrum P3 (Ray and Patankar 2001)

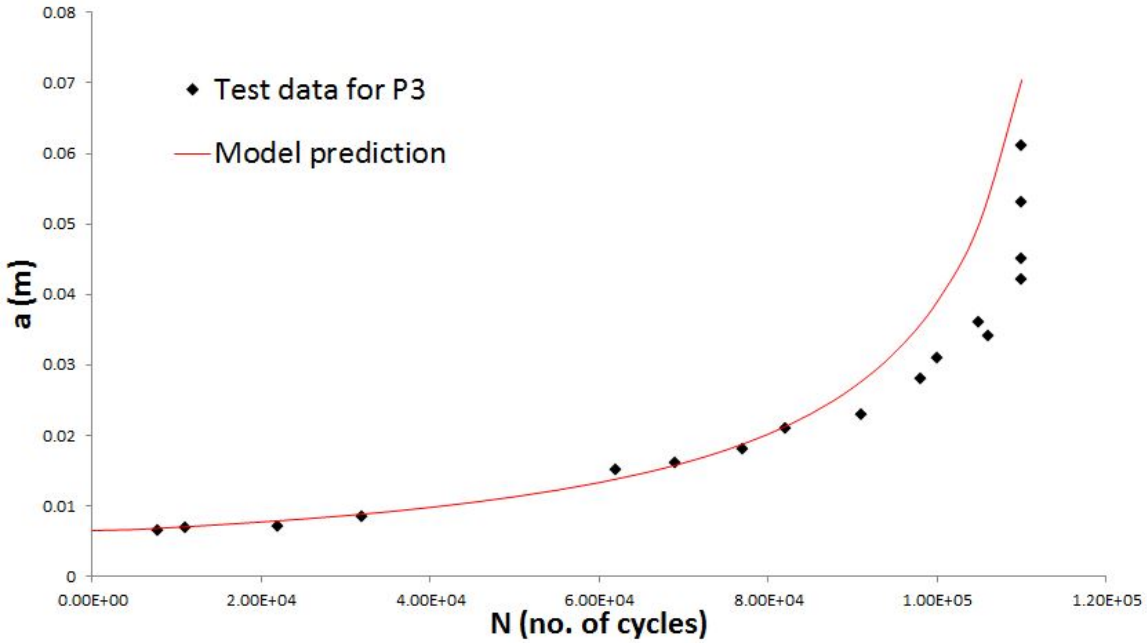

Figure 46. Comparison of predicted results with the test data of Al2024-T3

Chapter 4

CONCLUSION AND FUTURE WORK

4.1 Conclusion

The previously developed small time scale fatigue crack growth model for constant amplitude under positive stress ratio has been extended and modified in order to account for constant amplitude loading under negative stress ratio. This goal has been accomplished through an investigation of crack closure under negative stress ratio for different materials. An empirical model for crack opening stress is proposed in the present paper to quantify the influence of loading parameters and the material yield strength on plasticity induced crack closure. The crack opening level was defined as a function of σ_{max} and σ_{min}. Yield stress σ_y was included in the model to account for material effect for negative stress ratio. The proposed model has been compared with several literature models for crack closure. The proposed model was applied to literature results of fatigue crack growth rate and was able to collapse $da/dN - \Delta K_{eq}$ for a wide range of materials.

From the analysis and validation carried out, the following conclusions can be drawn:

- The modal parameters A and B for the small time scale model can be estimated using the paris model constants C and m for stress ratio R = 0.
- The compressive portion of the load cycle has a significant effect on plasticity induced crack closure. The crack opening stress decreases with decrease in the

stress ratio. This was found to be associated with the increase in reversed plastic deformation at the crack tip due to global crack contact.

- Literature results of da/dN-ΔK for negative stress ratios were analysed using the proposed crack closure model. The introduction of a scaling parameter β that accounts for the global contact stress level, was able to collapse the curves, indicating its applicability to explain the effect of negatice stress ratio.

While many engineering structures are always subjected to complex loading histories in service, the load interaction effects can occur as a result of the variable amplitude loading and affect the overall fatigue life. In the present research work, a study has been executed based on the previous work and the applicability of the improved small time scale model has been extended to the category of variable amplitude loading by implementing plasticity induced crack closure phenomena. Then the qualitative analysis has been carried out to investigate the performance capacity of the improved small time scale model. Finally, model predictions and the experimental data have been compared in the various load cases, including single, multiple overloads, underloads, combination of overload and underload and block loading.

From the analysis carried out, the following conclusions can be drawn:

- The main idea in the improved model under VA loading is based on the concept that the load interaction effect is due to changes in crack opening stress. Crack opening stress under VA loading is derived using virtual crack annealing method.
- A good agreement between the predicted curves and the test data is observed, which validates that the improved small time scale model has a good capability to predict crack growth rate under variable amplitude loading involving some basic loading spectra.

- The fatigue crack growth retardation or acceleration effect can be well simulated by fixing a relevant sensitivity parameter γ.

4.2 Future Work

The following suggestions are recommended for future investigations in order to better understand the crack growth response under several other load scenarios.

- It has been shown that the material yield strength affects the proposed "scaling parameter β". It would be worthwhile to investigate the influence of other parameters such as maximum applied stress etc.. that may affect the scaling parameter.
- The great difference of the values of sensitivity parameter γ, for different materials raises under different load magnitude raises a question whether the parameter is a material constant or a loading sequence variable. This will be investigated in the near future by comparing the values of γ for the same material under various loading sequences.
- The model's capability to simulate fatigue crack growth rate under any random amplitude load history should be further investigated by applying under random stress histories with noises, aircraft spectrum loading etc...
- Fatigue crack growth rate behaves differently under different environmental conditions. This could be further investigated and implemented in the small time scale model.

REFERENCES

Antunes, FV, L Correia, D Camas, and R Branco. 2015. "Effect of compressive loads on plasticity induced crack closure." *Theoretical and Applied Fracture Mechanics* 80:193–204.

Bannantine, Julie. 1990. "Fundamentals of metal fatigue analysis." *Prentice Hall, 1990,* 273.

Belnoue, Jonathan P, Tea-Sung Jun, Felix Hofmann, Brian Abbey, and Alexander M Korsunsky. 2010. "Evaluation of the overload effect on fatigue crack growth with the help of synchrotron XRD strain mapping." *Engineering Fracture Mechanics* 77 (16): 3216–3226.

Chen, Jingjie, Yi Huang, Leilei Dong, and Yugang Li. 2015. "A study on evaluation method of crack tip reverse plastic zone size for the center cracked steel plate model under tension–compression cyclic loading." *Engineering Fracture Mechanics* 133:138–151.

Christensen, RH. 1959. "Fatigue crack, fatigue damage and their detection." *Metal fatigue. New York: MacGraw-Hill.*

Elber, Wolf. 1997. "Fatigue crack closure under cyclic tension."

Forman, RG, V Shivakumar, JW Cardinal, LC Williams, and PC McKeighan. 2005. *Fatigue Crack Growth Database for Damage Tolerance Analysis, US Department of Transportation Federal Aviation Administration (FAA), Office of Aviation Research Washington, DC 20591.* Technical report. Final Report No. DOT/FAA/AR-05/15.

Huang, Xiaoping, Moan Torgeir, and Weicheng Cui. 2008. "An engineering model of fatigue crack growth under variable amplitude loading." *International Journal of Fatigue* 30 (1): 2–10.

Kumar, Raghuvir. 1995. "Influence of stress ratio on fatigue crack growth in mild steel." *Engineering Fracture Mechanics* 50 (3): 377–384.

Lang, M. 2000. "A model for fatigue crack growth, part II: modelling." *Fatigue and Fracture of Engineering Materials and Structures* 23 (7): 603–618.

Lee, Ouk Sub, and Zhi Wei Chen. 2002. "Improvement to Crack Retardation Models Using" Interactive Zone Concept"." *International Journal of Precision Engineering and Manufacturing* 3 (4): 72–77.

Liu, Yongming, Zizi Lu, and Jifeng Xu. 2012. "A simple analytical crack tip opening displacement approximation under random variable loadings." *International journal of fracture* 173 (2): 189–201.

Lu, Zizi, and Yongming Liu. 2010. "Small time scale fatigue crack growth analysis." *International Journal of Fatigue* 32 (8): 1306–1321.

Mehrzadi, Morteza. 2013. "FATIGUE CHARACTERIZATION OF AM60B MAGNESIUM ALLOY SUBJECTED TO CONSTANT AND VARIABLE AMPLITUDE LOADING WITH POSITIVE AND NEGATIVE STRESS RATIOS."

Mehrzadi, Morteza, and Farid Taheri. 2012. "The influence of negative and positive stress ratios on crack growth rate in AM60B magnesium alloy." *Materials Science and Engineering: A* 545:68–77.

———. 2013. "Influence of compressive cyclic loading on crack propagation in AM60B magnesium alloy under random and constant amplitude cyclic loadings." *Engineering Fracture Mechanics* 99:1–17.

Murthy, A Rama Chandra, GS Palani, and Nagesh R Iyer. 2007. "Remaining life prediction of cracked stiffened panels under constant and variable amplitude loading." *International journal of fatigue* 29 (6): 1125–1139.

Murthy, A Rama Chandra, GS Palani, and NR Iyer. 2004. "State-of-the-art review on fatigue crack growth analysis under variable amplitude loading." *Journal of the Institution of Engineers. India. Civil Engineering Division* 85 (aout): 118–129.

Newman Jr, JC. 1997. "Prediction of crack growth under variable-amplitude loading in thin-sheet 2024-T3 aluminum alloys."

Newman, JC. 1982. "Prediction of fatigue crack growth under variable-amplitude and spectrum loading using a closure model." In *Design of Fatigue and Fracture Resistant Structures.* ASTM International.

Newman, Jr JC. 1984. "A crack opening stress equation for fatigue crack growth." *International Journal of Fracture* 24 (4): R131–R135.

Padmadinata, Utama Herawan. 1990. "Investigation of crack-closure prediction models for fatigue in aluminum alloy sheet under flight-simulation loading." PhD diss., TU Delft, Delft University of Technology.

Paris, Paul C, and F Erdogan. 1997. "A critical analysis of crack propagation laws."

Porter, Theodore R. 1972. "Method of analysis and prediction for variable amplitude fatigue crack growth." *Engineering Fracture Mechanics* 4 (4): 717–736.

Ray, Asok, and Ravindra Patankar. 2001. "Fatigue crack growth under variable-amplitude loading: Part II–Code development and model validation." *Applied Mathematical Modelling* 25 (11): 995–1013.

RL, C. 1998. "Predicting the effects of load ratio on the fatigue crack growth rate and fatigue threshold." *Fatigue & Fracture of Engineering Materials & Structures* 21:411–423.

Rushton, PA, and F Taheri. 2003. "Prediction of crack growth in 350WT steel subjected to constant amplitude with overand under-loads using a modified wheeler approach." *Marine Structures* 16 (7): 517–539.

Sadananda, K, and AK Vasudevan. 2003. "Fatigue crack growth mechanisms in steels." *International Journal of Fatigue* 25 (9): 899–914.

Schijve, J. 1981. "Some formulas for the crack opening stress level." *Engineering Fracture Mechanics* 14 (3): 461–465.

Schijve, J, and D Broek. 1962. "The results of a test programme based on a gust spectrum with variable amplitude loading." *Aircraft Engng* 34:314–316.

Suresh, Subra. 1998. *Fatigue of materials.* Cambridge university press.

Walker, K. 1970. "The effect of stress ratio during crack propagation and fatigue for 2024-T3 and 7075-T6 aluminum." In *Effects of environment and complex load history on fatigue life.* ASTM International.

Wheeler, Orville Eugene. 1972. "Spectrum loading and crack growth." *Journal of basic engineering* 94 (1): 181–186.

Willenborg, James, RM Engle, and HA Wood. 1971. *A crack growth retardation model using an effective stress concept.* Technical report. DTIC Document.

Yang, Jian, Wei Zhang, and Yongming Liu. 2014. "Existence and insufficiency of the crack closure for fatigue crack growth analysis." *International Journal of Fatigue* 62:144–153.

Yuen, BKC, and F Taheri. 2006. "Proposed modifications to the Wheeler retardation model for multiple overloading fatigue life prediction." *International journal of fatigue* 28 (12): 1803–1819.

Zhang, Jia-zhen, XD He, and SY Du. 2007. "Analysis of the effects of compressive stresses on fatigue crack propagation rate." *International Journal of Fatigue* 29 (9): 1751–1756.

Zhang, Jia-zhen, XD He, Yu Sha, and SY Du. 2010. "The compressive stress effect on fatigue crack growth under tension–compression loading." *International Journal of Fatigue* 32 (2): 361–367.

Zhang, Junhong, Shuo Yang, and Jiewei Lin. 2015. "Fatigue crack growth rate of Ti-6Al-4V considering the effects of fracture toughness and crack closure." *Chinese Journal of Mechanical Engineering* 28 (2): 409–415.

Zhang, S, R Marissen, K Schulte, KK Trautmann, H Nowack, and J Schijve. 1987. "Crack propagation studies on Al 7475 on the basis of constant amplitude and selective variable amplitude loading histories." *Fatigue & fracture of engineering materials & structures* 10 (4): 315–332.

Zhang, Wei, and Yongming Liu. 2012. "In situ SEM testing for crack closure investigation and virtual crack annealing model development." *International Journal of Fatigue* 43:188–196.

Zhao, Tianwen, Jixi Zhang, and Yanyao Jiang. 2008. "A study of fatigue crack growth of 7075-T651 aluminum alloy." *International Journal of Fatigue* 30 (7): 1169–1180.